

Worm Monte Carlo study of the honeycomb-lattice loop model

Qingquan Liu^a, Youjin Deng^{a,*}, Timothy M. Garoni^b

^a*Hefei National Laboratory for Physical Sciences at Microscale,
Department of Modern Physics, University of Science and Technology of China,
Hefei, 230027, China*

^b*ARC Centre of Excellence for Mathematics and Statistics of Complex Systems,
Department of Mathematics and Statistics, The University of Melbourne,
Victoria 3010, Australia*

Abstract

We present a Markov-chain Monte Carlo algorithm of *worm* type that correctly simulates the $O(n)$ loop model on any (finite and connected) bipartite cubic graph, for any real $n > 0$, and any edge weight, including the fully-packed limit of infinite edge weight. Furthermore, we prove rigorously that the algorithm is ergodic and has the correct stationary distribution. We emphasize that by using known exact mappings when $n = 2$, this algorithm can be used to simulate a number of zero-temperature Potts antiferromagnets for which the Wang-Swendsen-Kotecký cluster algorithm is non-ergodic, including the 3-state model on the kagome lattice and the 4-state model on the triangular lattice. We then use this worm algorithm to perform a systematic study of the honeycomb-lattice loop model as a function of $n \leq 2$, on the critical line and in the densely-packed and fully-packed phases. By comparing our numerical results with Coulomb gas theory, we identify a set of exact expressions for scaling exponents governing some fundamental geometric and dynamic observables. In particular, we show that for all $n \leq 2$, the scaling of a certain return time in the worm dynamics is governed by the magnetic dimension of the loop model, thus providing a concrete dynamical interpretation of this exponent. The case $n > 2$ is also considered, and we confirm the existence of a phase transition in the 3-state Potts universality class that was recently observed via numerical transfer matrix calculations.

Keywords: Monte Carlo; Worm algorithm; Loop model

PACS: 02.70.Tt, 05.10.Ln, 64.60.De, 64.60.F-

1. Introduction

Among the myriad of models studied in the theory of critical phenomena, two fundamental examples that continue to play a central role are the q -state Potts model [1, 2, 3], and the $O(n)$ spin model [4, 5]. In the original spin representation, the parameter q or n must be a positive integer. However, the Fortuin-Kasteleyn representation [6] of the ferromagnetic Potts model and the loop representation [7] of the $O(n)$ spin model show how these models can be extended to arbitrary

*Corresponding author

Email addresses: liuqq@mail.ustc.edu.cn (Qingquan Liu), yjdeng@ustc.edu.cn (Youjin Deng), t.garoni@ms.unimelb.edu.au (Timothy M. Garoni)

Preprint submitted to Nuclear Physics B

March 29, 2018

real $q, n \geq 0$, by re-expressing them as models of random geometric objects: clusters or loops, respectively. In fact, the extension of the Potts model to non-integer q can also be formulated directly in the spin language, by re-expressing the Potts spin clusters in terms of domain walls [8]. These geometric models play a major role in recent developments of conformal field theory [9] via their connection with Schramm-Loewner evolution (SLE) [10, 11].

Monte Carlo methods are an indispensable tool in statistical mechanics [12, 13]. The Sweeny algorithm [14] and the Swendsen-Wang-Chayes-Machta cluster-algorithm [15, 16] provide remarkably efficient [17, 18] tools for studying the ferromagnetic Potts (random-cluster [19]) model, and are valid for any real $q > 0$, or $q > 1$, respectively. For loop models, by contrast, efficient simulation at noninteger n has posed a significant challenge. Instead, numerical transfer-matrix techniques have typically been used [20, 21]. Monte Carlo simulations at $n \neq 1$ have been reported in [22, 23], however the algorithms used were essentially single-spin-flip Metropolis algorithms for Ising spins on the dual lattice. As such, their efficiency is limited, and they are manifestly non-ergodic¹ at infinite edge weight. In [24], a cluster algorithm was presented that is valid for all $n \geq 1$, which is dramatically more efficient than the single-spin-flip algorithms on the critical line. However, its efficiency deteriorates rapidly as the edge weight increases, and it too becomes non-ergodic at infinite edge weight.

In [25], a Monte Carlo algorithm of *worm* type for simulating the honeycomb-lattice fully-packed loop model with $n = 1$ was presented, and its validity was rigorously proved. In this article, we present a worm algorithm that correctly simulates the $O(n)$ loop model on any bipartite cubic graph,² for any real $n > 0$, and any edge weight, including the fully-packed limit of infinite edge weight. Furthermore, we prove rigorously that the algorithm is ergodic and has the correct stationary distribution. We then use this algorithm to perform a systematic study of the honeycomb-lattice loop model as a function of n . By comparing our numerical results for $n \leq 2$ with Coulomb-gas theory [26], we identify the exact scaling exponents of some fundamental geometric observables, as well as certain observables related to dual Ising spins. Furthermore, we find that for all $n \leq 2$, the scaling dimension of a certain very natural return time in the worm dynamics coincides precisely with the magnetic dimension of the loop model, which provides a concrete dynamical interpretation of this exponent which is meaningful for both integer and non-integer n . See section 3. We also study the case $n > 2$, and confirm the existence of a critical transition in the 3-state Potts universality class, which was recently observed using transfer matrices [21]. While the honeycomb-lattice model is perhaps the archetypal loop model, and is certainly the most well-studied case, there are other examples of bipartite cubic graphs which are of interest, including the $(4 \cdot 8^2)$ Archimedean lattice (dual of the Union Jack lattice), and the Hydrogen-peroxide lattice (which is three-dimensional). Systematic studies of the loop models on both of these lattices can be performed using the algorithms described in this article; the results will be presented elsewhere.

In addition to the study of loop models, the worm algorithms that we present here can also be applied to the study of a number of antiferromagnetic Potts models. It is well known that the honeycomb-lattice fully-packed loop model with $n = 1$ is equivalent to the zero-temperature triangular-lattice antiferromagnetic Ising model. The latter model (which is critical) provides a canonical example of geometric frustration, but is notoriously difficult to simulate. In fact, even

¹Following the typical usage in the physics literature, we take *ergodic* as synonymous with *irreducible*. Recall that a Markov chain is irreducible if for each pair of states i and j there is a positive probability that starting in i we eventually visit j , and vice versa.

²All graphs considered in this article are implicitly assumed to be finite and connected.

the most sophisticated tailor-made cluster algorithms [27, 28] are thought to be non-ergodic. However, the worm algorithm constructed in [25] immediately provides a provably ergodic Monte Carlo method for this problem. Furthermore, it is known that the honeycomb-lattice fully-packed loop model with $n = 2$ is equivalent to both the zero-temperature kagome-lattice 3-state Potts antiferromagnet and the zero-temperature triangular-lattice 4-state Potts antiferromagnet [29]. Both of these models are believed to be critical. While the Wang-Swendsen-Kotecký [30] (WSK) cluster algorithm is undoubtedly the current state-of-the-art for simulating antiferromagnetic Potts models, it has recently been proved [31, 32] to be non-ergodic for both of these cases. By contrast, the worm algorithms described in Section 2 have been proved to be ergodic and can be applied in a straightforward way to the study of both of these Potts antiferromagnets. The details of this application will be reported elsewhere (but see also Section 4 for further discussion).

Worm algorithms were first applied to classical lattice models in [33], and it was demonstrated empirically in [34] that the worm algorithm is an extraordinarily efficient method for simulating the three-dimensional Ising model. See [35, 36] for some recent applications to $O(n)$ models. Worm algorithms provide a natural way to simulate *cycle-space* models. Given a finite graph $G = (V, E)$, the cycle space, $C(G)$, is the set of all $A \subseteq E$ such that every vertex in the spanning subgraph (V, A) is even. We call $A \subseteq E$ and (V, A) *Eulerian* whenever $A \in C(G)$. Fig. 1(a) shows a typical configuration on the honeycomb lattice. The essence of the worm idea is to enlarge the state space $C(G)$ to include a pair of *defects* (i.e., vertices of odd degree), and then to move these defects via random walk. When the two defects collide, the configuration becomes Eulerian once more. A very natural class of cycle-space models is defined for $n, x > 0$ by the probability measure

$$\phi_{G,n,x}(A) \propto n^{c(A)} x^{|A|}, \quad A \in C(G), \quad (1)$$

where $c(A)$ is the cyclomatic number of the spanning subgraph (V, A) . The cyclomatic number of a graph is simply the minimum number of edges to remove from it in order to make it cycle-free. On graphs G of maximum degree $\Delta(G) \leq 3$ therefore, all $A \in C(G)$ consist of a collection of disjoint cycles, or *loops*, and $c(A)$ is then simply the number of such loops. Consequently, the model (1) is typically referred to as the *loop model*, and bipartite cubic graphs (such as the honeycomb lattice) provide a natural setting for its study.

It is well known [7] that on any graph $G = (V, E)$ of maximum degree $\Delta(G) \leq 3$, the model (1) arises for positive integer n as a loop representation of an n -component spin model,

$$Z = \text{Tr} \prod_{ij \in E} (1 + n x \sigma_i \cdot \sigma_j), \quad (2)$$

where $\sigma = (\sigma^1, \dots, \sigma^n) \in \mathbb{R}^n$ and Tr denotes normalized integration with respect to any *a priori* measure $\langle \cdot \rangle_0$ on \mathbb{R}^n satisfying $\langle \sigma^\alpha \sigma^\beta \rangle_0 = \delta_{\alpha,\beta}/n$ and $\langle \sigma^\alpha \rangle_0 = \langle \sigma^\alpha \sigma^\beta \sigma^\gamma \rangle_0 = 0$. In particular, uniform measure on the unit sphere is allowed, as are various *face-cubic* and *corner-cubic* measures [7]. For $n \neq 1$, the Boltzmann weight (2) with spins on a sphere defines a nonstandard $O(n)$ spin model, which has positive weights only for $|x| < 1/n$, but it is, nevertheless, expected to belong to the usual $O(n)$ universality class.

In the limit $x \rightarrow +\infty$, the support of $\phi_{G,n,x}$ reduces to the set of all $A \in C(G)$ with maximal $|A|$. On bipartite cubic graphs $\max_{A \in C(G)} |A| = |V|$, so the set of all such *fully-packed* configurations is simply

$$\mathcal{F}(G) := \{A \in C(G) : d_v(A) = 2 \text{ for all } v \in V\}. \quad (3)$$

Figure 1: Typical loop configuration (a) and fully-packed loop configuration (b) on the honeycomb lattice with periodic boundary conditions. Thick lines denote occupied edges, thin lines denote vacant edges.

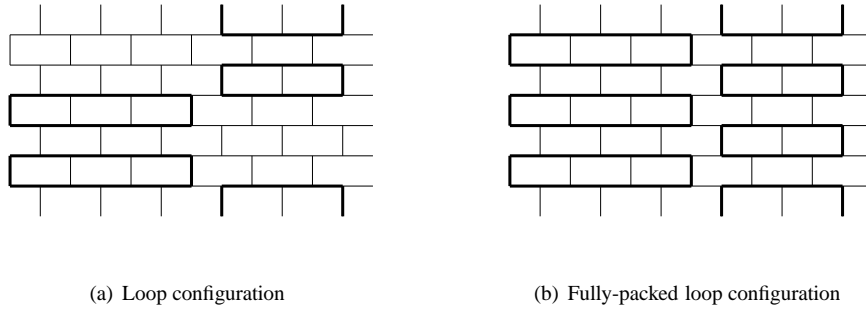


Fig. 1(b) shows a typical fully-packed configuration on the honeycomb lattice. We note that the elements of $\mathcal{F}(G)$ are referred to as *2-factors*³ by graph theorists [37]. We also remark that $A \in \mathcal{F}(G)$ iff $E \setminus A$ is a dimer covering (perfect matching) of G . Finally, we note that the limiting measure is simply

$$\phi_{G,n}(A) := \phi_{G,n,\infty}(A) \propto n^{c(A)}, \quad A \in \mathcal{F}(G).$$

A great deal is known about the loop model (1) on the honeycomb lattice when $n \leq 2$. For given n , the model is believed to have three distinct phases: a disordered phase (small x), a densely-packed (DP) phase (large finite x), and a fully-packed (FP) phase (infinite x). Furthermore, the model is exactly solvable [38, 39, 40, 41, 42] on the curves

$$x = \frac{1}{\sqrt{2 \pm \sqrt{2-n}}}. \quad (4)$$

The plus sign in (4) corresponds to the critical curve, $x_c(n)$, separating the disordered and densely-packed phases [43]. The minus sign in (4) corresponds to a curve of stable fixed points in the densely-packed phase. For all finite $x > x_c$, the loop model is in the densely-packed phase, which is critical [20]. The fully-packed model is also critical, however it is known to be in a distinct universality class to the densely-packed phase [44, 45, 46]. For convenience, we shall refer to the model (1) with $x_c < x < \infty$ as the densely-packed loop (DPL) model, and to the $x = \infty$ model as the fully-packed loop (FPL) model.

The loop model with loop fugacity n can be related to a Coulomb gas [26, 46] with coupling g by

$$n = -2 \cos(\pi g/4), \quad (5)$$

with

$$g \in \begin{cases} [2, 4], & x_c < x \leq +\infty, \\ [4, 6], & x = x_c. \end{cases} \quad (6)$$

³More precisely, if $A \in \mathcal{F}(G)$ then the spanning subgraph (V, A) is a 2-factor.

Recall [47] that the critical (densely-packed) loop model with $0 \leq n \leq 2$ corresponds to a tricritical (critical) Potts model with $q = n^2$. The normalization for g given in (5) and (6), which is a factor of 4 times larger than the g presented in [26], is in fact the standard normalization for the Coulomb gas corresponding to the $q = n^2$ Potts model, rather than the $O(n)$ loop model. This choice facilitates easy translation between loop and Potts exponents, which will prove convenient in Section 3.

Coulomb gas theory [26] predicts a whole spectrum of exact scaling dimensions characterizing the loop model. However, we emphasize that identifying *which* loop-model observables these exponents actually govern is not always obvious. In [24], Monte Carlo simulations were combined with Coulomb gas predictions to identify the exact scaling exponents for a number of natural geometric observables, as well as observables related to dual Ising spins. The results presented in [24], however, were restricted to the critical branch, $x = x_c$, and to $n \geq 1$. In this work we shall use worm algorithms to extend these observations to all $n > 0$, and to the DP and FP phases. See Section 3.

The outline of this article is as follows. The necessary theoretical results concerning the algorithms appear in Section 2. In Section 3 we then present our numerical results for the $n \leq 2$ honeycomb-lattice loop model in the critical, densely-packed, and fully-packed phases, and also for the $n > 2$ model. Section 4 then concludes with a discussion.

2. Worm dynamics for loop models

We begin our discussion of worm dynamics by constructing a worm algorithm to simulate (1) on an arbitrary graph, for any $0 < n, x < \infty$. This essentially generalizes the presentation in [34, 25] to include a loop fugacity in the stationary distribution. We then demonstrate that it is possible to make this algorithm *rejection-free*, in a certain sense. We then turn our attention to the specific case of cubic graphs, and consider the limit $x \rightarrow \infty$. In particular, we rigorously prove that the rejection-free worm algorithm on any bipartite cubic graph remains ergodic at $x = +\infty$.

2.1. Simple worm dynamics

Fix a finite graph $G = (V, E)$, and for any $A \subseteq E$ let $\partial A \subseteq V$ denote the set of all vertices which have odd degree in the spanning subgraph (V, A) . Loosely, ∂A is just the set of sites that *touch* an odd number of the bonds in the bond configuration A . If $u, v \in V$ are distinct we write

$$\mathcal{S}_{u,v}(G) := \{A \subseteq E : \partial A = \{u, v\}\},$$

and

$$\mathcal{S}_{v,v}(G) := \{A \subseteq E : \partial A = \emptyset\}.$$

We emphasize that $\mathcal{S}_{v,v}(G) = C(G)$ for every $v \in V$. We take the state space of the worm algorithm to be

$$\mathcal{S}(G) := \{(A, u, v) : u, v \in V \text{ and } A \in \mathcal{S}_{u,v}(G)\},$$

i.e., all ordered triples (A, u, v) with $A \subseteq E$ and $u, v \in V$, such that $A \in \mathcal{S}_{u,v}(G)$. Note that if $(A, u, v) \in \mathcal{S}(G)$ then $A \in C(G)$ iff $u = v$. Thus, the bond configurations allowed in the state space of the worm algorithm constitute a superset of the Eulerian configurations. Finally, we assign probabilities to the configurations in $\mathcal{S}(G)$ according to

$$\pi_{G,n,x}(A, u, v) \propto d_u d_v n^{c(A)} x^{|\partial A|}, \quad (A, u, v) \in \mathcal{S}(G), \quad (7)$$

where d_v denotes the degree in G of $v \in V$. In the following, when we wish to refer to the degree of $v \in V$ in the spanning subgraph (V, A) we will write $d_v(A)$. Loosely, $d_v(A)$ is simply the number of bonds that touch v in the bond configuration A . In this notation we have $d_v = d_v(E)$.

The first step in constructing the standard worm algorithm is to consider the worm *proposal matrix*, $P^{(0)}$, which is defined for all $uu' \in E$ and $v \in V$ by

$$P^{(0)}[(A, u, v) \rightarrow (A \Delta uu', u', v)] = P^{(0)}[(A, v, u) \rightarrow (A \Delta uu', v, u')] = \frac{1}{2d_u}, \quad (8)$$

all other entries being zero. Here Δ denotes symmetric difference, i.e. delete the bond uu' from A if it is present, or insert it if it is absent. It is easy to see that $P^{(0)}$ is an ergodic transition matrix on $\mathcal{S}(G)$. According to (8), the moves proposed by the worm algorithm are as follows: Pick uniformly at random one of the two defects (say, u) and one of the edges emanating from u (say, uu'), then move from the current configuration (A, u, v) to the new configuration $(A \Delta uu', u', v)$.

Now we simply apply the usual Metropolis-Hastings prescription (see e.g. [13]) to assign acceptance probabilities to the moves proposed by $P^{(0)}$, so that the resulting transition matrix, $P_{G,n,x}$, is in detailed balance with (7). Explicitly, for all $uu' \in E$ and $v \in V$ we have

$$\begin{aligned} P_{G,n,x}[(A, u, v) \rightarrow (A \Delta uu', u', v)] &= P_{G,n,x}[(A, v, u) \rightarrow (A \Delta uu', v, u')] \\ &= \frac{1}{2d_u} \begin{cases} \min(1, xn) & uu' \notin A \text{ and } u \leftrightarrow u' \text{ in } (V, A) \\ \min(1, x) & uu' \notin A \text{ and } u \nleftrightarrow u' \text{ in } (V, A) \\ \min(1, 1/nx) & uu' \in A \text{ and } u \leftrightarrow u' \text{ in } (V, A \setminus uu') \\ \min(1, 1/x) & uu' \in A \text{ and } u \nleftrightarrow u' \text{ in } (V, A \setminus uu') \end{cases} \quad (9) \end{aligned}$$

The notation $u \leftrightarrow u'$ in (9) means that vertices u and u' are connected in the stated spanning subgraph of G . The transitions (9) define $P_{G,n,x}$ uniquely since all other transitions occur with zero probability, except the identity transitions $(A, u, v) \rightarrow (A, u, v)$, whose transition probabilities are fixed by normalization.

Now let us return to our original goal, which was to sample from $\mathcal{C}(G)$. As elaborated below in Lemma 2.1, achieving this is as simple as running the worm chain and choosing to only measure observables when the two defects meet, $u = v$. This defines an ergodic Markov sub-chain on

$$\{(A, u, v) \in \mathcal{S}(G) : u = v\} \cong \mathcal{C}(G) \times V \quad (10)$$

with stationary distribution $\bar{\pi}_{G,n,x}(A, v) \propto n^{c(A)} x^{|A|}$, and therefore for any loop-model observable $X : \mathcal{C}(G) \rightarrow \mathbb{R}$ we have $\langle X \rangle_{\bar{\pi}_{G,n,x}} = \langle X \rangle_{\phi_{G,n,x}}$.

The resulting Monte Carlo algorithm is summarized in Algorithm 1. Note that the acceptance probabilities (which are simply $2d_u P_{G,n,x}[(A, u, v) \rightarrow (A \Delta uu', u', v)]$) will in general depend on the topology of the loops in a non-trivial way; we shall return to this point in Section 2.6. The abbreviation UAR simply means *uniformly at random*.

Remark 2.1. The naive $n \rightarrow 0$ limit of (1) with $x < \infty$ held fixed reduces to a trivial measure concentrated on the single state $A = \emptyset$, and the naive $n \rightarrow 0$ limit of Algorithm 1 leads to a trivial dynamics which correctly simulates this trivial model. Non-trivial $n \rightarrow 0$ limits can be taken however; for example, conditioning on positive cyclomatic number before taking the $n \rightarrow 0$ limit of (1) yields a model of self-avoiding polygons. Worm dynamics can be developed to simulate both self-avoiding walks and self-avoiding polygons, however a discussion of these issues would lead us too far afield here. A discussion of such algorithms will be reported elsewhere.

Algorithm 1 (Simple worm algorithm).

loop

Current state is (A, u, v)

UAR, pick one of the two defects (say u)

UAR, pick a neighbor u' of u

Make the transition $(A, u, v) \rightarrow (A\Delta uu', u', v)$ with acceptance probability inferred from (9)

if $u' = v$ **then**

Measure observables

end if

end loop

2.2. Markov sub-chains

Let us pause momentarily, and consider, quite generally, that we have an ergodic Markov chain on a finite state space \mathcal{S} which is in detailed balance with a distribution π , and suppose that we only observe the process when it is in a state in $\mathcal{X} \subset \mathcal{S}$. This new process is a Markov chain on \mathcal{X} with transition matrix

$$(\bar{P})_{ss'} := (P)_{ss'} + \sum_{n=0}^{\infty} \sum_{s_0, s_1, \dots, s_n \in \bar{\mathcal{X}}} (P)_{ss_0} \prod_{l=1}^n (P)_{s_{l-1}s_l} (P)_{s_n s'}.$$

Lemma 2.1. \bar{P} is ergodic and in detailed balance with the restriction of π to \mathcal{X}

$$\bar{\pi}_s = \frac{\pi_s}{\sum_{s' \in \mathcal{X}} \pi_{s'}}, \quad s \in \mathcal{X}.$$

Proof. The ergodicity of \bar{P} on \mathcal{X} follows immediately from the ergodicity of P on \mathcal{S} , and one can easily verify directly that \bar{P} is in detailed balance with $\bar{\pi}$ by using the fact that P is in detailed balance with π . \square

We now wish to make the following observation. Since we only observe the \mathcal{S} -chain when it visits $\mathcal{X} \subset \mathcal{S}$, we have quite a bit of freedom to modify the transition probabilities in $\bar{\mathcal{X}} = \mathcal{S} \setminus \mathcal{X}$ without affecting the stationary distribution of the \mathcal{X} -chain. In particular, we can forbid identity transitions in $\bar{\mathcal{X}}$.

Corollary 2.2. *If*

$$(P')_{ss'} := \begin{cases} (P)_{ss'} & s \in \mathcal{X} \\ (P)_{ss'} & s \in \bar{\mathcal{X}}, s' \neq s \\ \frac{(P)_{ss'}}{1 - (P)_{ss}} & s \in \bar{\mathcal{X}}, s' = s \\ 0 & s \in \bar{\mathcal{X}}, s' = s \end{cases}$$

then \bar{P}' is in detailed balance with $\bar{\pi}$.

Proof. It is elementary to verify directly that P' is in detailed balance with

$$\pi'_s = \begin{cases} \pi_s & s \in \mathcal{X}, \\ (1 - (P)_{ss}) \pi_s & s \in \bar{\mathcal{X}}. \end{cases}$$

Lemma 2.1 then immediately implies that \bar{P}' is in detailed balance with $\bar{\pi}$. \square

Therefore, both \bar{P} and \bar{P}' are in detailed balance with the same distribution $\bar{\pi}$. Since P' forbids identity transitions $s \rightarrow s$ when $s \in \bar{\mathcal{X}}$ (which correspond to rejections in the context of Metropolis algorithms) P' is clearly more efficient than P at sampling from \mathcal{X} . We shall refer to P' as a rejection-free chain, although it should be emphasized that rejections are still allowed inside \mathcal{X} .

A concrete example of the advantage of using the rejection-free chain is provided by considering worm algorithms for fully-packed loop models. Indeed, as we shall see, the $x \rightarrow \infty$ limit of $P_{G,n,x}$ is absorbing, while the corresponding rejection-free algorithm remains ergodic (at least on bipartite cubic graphs).

2.3. Rejection-free worm dynamics

Thus far we have glossed over an important issue, namely the ergodicity of $P_{G,n,x}$. It is not hard to see that $P_{G,n,x}$ is ergodic whenever $x < \infty$. However, $P_{G,n,x}$ is manifestly non-ergodic when $x = +\infty$, in fact it is absorbing. Indeed, as $x \rightarrow \infty$ the probabilities for transitions that remove an edge vanish. Consequently,

$$P_{n,+\infty}[(A, u, v) \rightarrow (A, u, v)] = 1 - \frac{d_u - d_u(A)}{2d_u} - \frac{d_v - d_v(A)}{2d_v},$$

and all states $(A, u, v) \in \mathcal{S}(G)$ for which both $d_u(A) = d_u$ and $d_v(A) = d_v$ become absorbing as $x \rightarrow \infty$.

Suppose now that G is k -regular. Then (A, u, v) will be absorbing when $x = +\infty$ iff $d_u(A) = d_v(A) = k$. By definition, if $(A, u, v) \in \mathcal{S}(G)$ then when $u = v$ the vertex degree $d_u(A) = d_v(A)$ is even, whereas when $u \neq v$ both $d_u(A)$ and $d_v(A)$ are odd. Thus, if k is odd then (A, u, v) can be absorbing only if $u \neq v$, and so all states with $A \in \mathcal{C}(G)$ remain non-absorbing. In particular, on a cubic graph we can now see that as $x \rightarrow \infty$ all states $(A, v, v) \in \mathcal{C}(G) \times V$ remain non-absorbing while all states (A, u, v) with $u \neq v$ and $d_u(A) = d_v(A) = 3$ become absorbing; once both defects have degree 3, the $P_{G,n,x}$ chain remains in the given state for eternity.

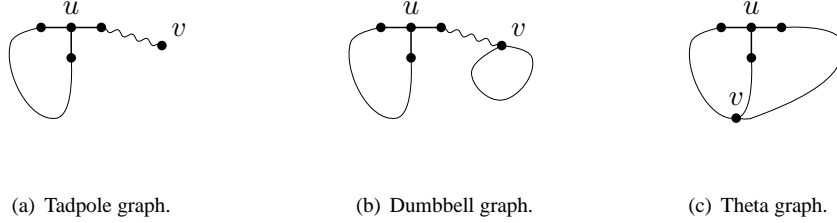
We cannot, therefore, use $P_{G,n,x}$ to simulate the fully-packed loop model. As we shall see, however, we can use its rejection-free counterpart. Following Corollary 2.2, we define a new transition matrix $P'_{G,n,x}$ by explicitly conditioning on making a non-trivial transition whenever $u \neq v$. Specifically, we define

$$\begin{aligned} P'_{G,n,x}[(A, u, v) \rightarrow (A\Delta uu', u', v)] &= P'_{G,n,x}[(A, v, u) \rightarrow (A\Delta uu', v, u')] \\ &= \begin{cases} P_{G,n,x}[(A, u, v) \rightarrow (A\Delta uu', u', v)] & u = v, \\ \frac{P_{G,n,x}[(A, u, v) \rightarrow (A\Delta uu', u', v)]}{1 - P_{G,n,x}[(A, u, v) \rightarrow (A, u, v)]} & u \neq v, \end{cases} \quad (11) \\ P'_{G,n,x}[(A, u, u) \rightarrow (A, u, u)] &= P_{G,n,x}[(A, u, u) \rightarrow (A, u, u)]. \end{aligned}$$

All other transitions occur with zero probability. In particular, no identity transitions are allowed from non-Eulerian states. Corollary 2.2 immediately implies that $P'_{G,n,x}$ can be used to simulate $\phi_{G,n,x}$ for any $0 < n, x < \infty$. We now proceed to show that in fact $P'_{G,n,x}$ remains valid even at $x = +\infty$.

Remark 2.2. While the explicit conditioning (11) is perhaps the simplest way to ensure ergodicity is retained as $x \rightarrow \infty$, there are variations of this idea that also work. Indeed, the algorithm

Figure 2: Possible topologies of the defect cluster $C_{uv}(A)$ when $d_u(A) = 3$.



presented in [25] for the $n = 1$ case was constructed in a slightly different way; the main consequence is that while configurations with $d_u(A) = d_v(A) = 1$ were allowed in [25], they are forbidden as $x \rightarrow \infty$ in the algorithm we present here, as we shall now see.

2.4. Worm dynamics for fully-packed loops on bipartite cubic graphs

We now consider the $x \rightarrow \infty$ limit of $P'_{G,n,x}$. We begin by noting that whenever G has maximum degree $\Delta(G) \leq 3$ there are only a small number of possible topologies that the connected components of states in $\mathcal{S}(G)$ can have (see Fig. 2).

Proposition 2.3. *Let G be a finite graph with $\Delta(G) \leq 3$, let $(A, u, v) \in \mathcal{S}(G)$, and let $C_{uv}(A)$ be the component containing u and v in (V, A) . Then all components other than $C_{uv}(A)$ are isolated vertices or cycles, and we have the following classification of the possible topologies of the component $C_{uv}(A)$*

$$C_{uv}(A) = \begin{cases} \text{isolated vertex} & d_u(A) = d_v(A) = 0 \\ \text{path} & d_u(A) = d_v(A) = 1 \\ \text{cycle} & d_u(A) = d_v(A) = 2 \\ \text{tadpole graph} & d_u(A) = 3, d_v(A) = 1 \text{ or } d_u(A) = 1, d_v(A) = 3 \\ \text{dumbbell or theta graph} & d_u(A) = d_v(A) = 3 \end{cases}$$

Proposition 2.3 is intuitively obvious and its proof (which we omit) is straightforward.

For the remainder of this section we shall restrict attention to bipartite cubic graphs. On such graphs, the limit as $x \rightarrow \infty$ of $P'_{G,n,x}$ is now easily seen to be given by

$$\begin{aligned} & \lim_{x \rightarrow \infty} P'_{G,n,x}[(A, u, v) \rightarrow (A \Delta uu', u', v)] \\ &= \begin{cases} 1/6 & u = v, uu' \notin A, \\ 1/4 & d_u(A) = d_v(A) = 1, uu' \notin A, \\ 1/2 & d_u(A) = 1, d_v(A) = 3, uu' \notin A, \\ 1/6 & C_{uv}(A) \text{ is a theta graph,} \\ n/2(n+2) & C_{uv}(A) \text{ is a dumbbell graph, } u \leftrightarrow u' \text{ in } (V, A \setminus uu'), \\ 1/2(n+2) & C_{uv}(A) \text{ is a dumbbell graph, } u \leftrightarrow u' \text{ in } (V, A \setminus uu'), \end{cases} \end{aligned} \quad (12)$$

and

$$\lim_{x \rightarrow \infty} P'_{G,n,x}[(A, u, u) \rightarrow (A, u, u)] = 2/3. \quad (13)$$

All other transitions occur with zero probability.

Now consider the subspace

$$\mathcal{R}(G) := \{(A, u, v) \in \mathcal{S}(G) : d_x(A) \neq 0 \text{ for all } x \text{ and } d_u(A) + d_v(A) \geq 4\}. \quad (14)$$

If $(A, u, v) \in \mathcal{R}(G)$, then either $|A| = |V|$ or $|A| = |V| + 1$. Furthermore, since (12) only allows the deletion of edges when $|A| = |V| + 1$, it is clear that

$$\lim_{x \rightarrow \infty} P'_{G,n,x}[(A, u, v) \rightarrow (A \Delta uu', u', v)] = 0$$

whenever $(A, u, v) \in \mathcal{R}(G)$ and $(A \Delta uu', u', v) \notin \mathcal{R}(G)$, so \mathcal{R} is closed (and therefore recurrent). The restriction of $P'_{G,n,\infty}$ to $\mathcal{R}(G)$ therefore defines a Markov chain on $\mathcal{R}(G)$. We emphasize that the set of all bond configurations A for which $(A, v, v) \in \mathcal{R}(G)$ corresponds precisely with $\mathcal{F}(G)$.

Remark 2.3. Since G is a bipartite cubic graph, we know that $|A| = |V|$ for all $A \in \mathcal{F}(G)$. It is therefore natural to consider $\lim_{x \rightarrow \infty} x^{-|V|} Z_{G,n,x} \pi'_{G,n,x}(A, u, v)$, where $Z_{G,n,x}$ is the appropriate normalization constant (partition function). It is straightforward to verify that this limiting measure is supported on $\mathcal{R}(G)$ and is detailed balance with (12).

Remark 2.4. The space $\mathcal{R}(G)$ given by (14) is strictly smaller than the state space of the worm dynamics considered in [25]. In particular, no states in which the defect cluster is a path are allowed in (14).

Before proceeding further, it is useful to note that $\mathcal{R}(G)$ has the disjoint partition $\mathcal{R}(G) = \mathcal{E} \cup \mathcal{T} \cup \Theta \cup \mathcal{D}$, where

$$\begin{aligned} \mathcal{E} &= \{(A, u, v) \in \mathcal{R}(G) : C_{uv}(A) \text{ is a cycle}\}, \\ \mathcal{T} &= \{(A, u, v) \in \mathcal{R}(G) : C_{uv}(A) \text{ is a tadpole graph}\}, \\ \Theta &= \{(A, u, v) \in \mathcal{R}(G) : C_{uv}(A) \text{ is a theta graph}\}, \\ \mathcal{D} &= \{(A, u, v) \in \mathcal{R}(G) : C_{uv}(A) \text{ is a dumbbell graph}\}. \end{aligned} \quad (15)$$

Now let us denote the restriction of (12) to $\mathcal{R}(G)$ by $P'_{G,n}$. From (12) we can see that the only transitions from $(A, u, u) \in \mathcal{E}$ which occur with non-zero probability are $(A, u, u) \rightarrow (A \cup uu', u', u)$ and $(A, u, u) \rightarrow (A \cup uu', u, u')$, which both occur with the same probability $1/6$, and the identity transition $(A, u, u) \rightarrow (A, u, u)$. We are therefore free to multiply the two transition probabilities $P'_{G,n}[(A, u, u) \rightarrow (A \Delta uu', u', u)] = 1/6$ from states $(A, u, u) \in \mathcal{E}$ by a constant factor $0 < \gamma \leq 3$, provided that we also redefine the probabilities for identity transitions, so that we retain correctly-normalized row sums. The only effect of such a modification is to multiply the stationary probabilities of all the states $(A, u, u) \in \mathcal{E}$ by the same constant $1/\gamma$. Therefore, such modifications do not affect detailed balance. If we now choose $\gamma = 3$, then the identity transitions from \mathcal{E} will occur with zero probability. We thus obtain an entirely rejection-free Monte Carlo method.

Putting all these details together, let us now define the following transition matrix $P_{G,n}$ on

$\mathcal{R}(G)$

$$\begin{aligned}
P_{G,n}[(A, u, v) \rightarrow (A \Delta uu', u', v)] &= P_{G,n}[(A, v, u) \rightarrow (A \Delta uu', v, u')] \\
&= \begin{cases} 1/2 & (A, u, v) \in \mathcal{E} \cup \mathcal{T} \text{ and } uu' \notin A, \\ 1/6 & (A, u, v) \in \Theta, \\ n/2(n+2) & (A, u, v) \in \mathcal{D} \text{ and } uu' \text{ is a bridge,} \\ 1/2(n+2) & (A, u, v) \in \mathcal{D} \text{ and } uu' \text{ is not a bridge.} \end{cases} \quad (16)
\end{aligned}$$

All other transitions are assigned zero probability; in particular, no identity transitions are allowed. The transition matrix $P_{G,n}$ corresponds to a very simple dynamics: if $|A| = |V|$ we must add one of the vacant edges incident to one of the defects; if $|A| = |V| + 1$ must delete one of the occupied edges incident to one of the defects.

Remark 2.5. Note that the only appearance of n in (16) occurs when $d_u(A) = d_v(A) = 3$. Loosely, (16) says that for transitions from degree 3 defects, the relative weight given by $P_{G,n}$ of traversing a bridge is n , while the relative weight of traversing a non-bridge is 1.

It is now elementary to show that $P_{G,n}$ is in detailed balance with the following distribution on $\mathcal{R}(G)$

$$\pi_{G,n}(A, u, v) = \frac{n^{c(A)}}{Z_n} \begin{cases} 1 & (A, u, v) \in \mathcal{E} \cup \mathcal{T}, \\ 3/n & (A, u, v) \in \Theta, \\ (n+2)/n & (A, u, v) \in \mathcal{D}. \end{cases} \quad (17)$$

We prove in the next section that $P_{G,n}$ is also ergodic. It then follows from (17) and Lemma 2.1 that $P_{G,n}$ defines a valid Markov-chain Monte Carlo algorithm to simulate the fully-packed loop model on any bipartite cubic graph. We summarize this algorithm in Algorithm 2.

Algorithm 2 (FPL worm algorithm).

loop

Current state is (A, u, v)

if $u = v$ **then**

Choose the unique edge $uu' \notin A$

Perform, UAR, either $(A, u, u) \rightarrow (A \cup uu', u', u)$ or $(A, u, u) \rightarrow (A \cup uu', u, u')$

else if $u \neq v$ **then**

if $d_u(A) = 1$ or $d_v(A) = 1$ (say u) **then**

Choose, UAR, one of the 2 vacant edges incident to u (say uu')

Make the transition $(A, u, v) \rightarrow (A \cup uu', u', v)$

else if $d_u(A) = d_v(A) = 3$ **then**

Choose, UAR, one of the 2 defects (say u)

Choose with probability $\mathbb{P}(u')$ one of the 3 neighbors of u (say u')

Make the transition $(A, u, v) \rightarrow (A \setminus uu', u', v)$

end if

end if

end loop

We note that the only place in which the topology for the loop configuration enters into

Algorithm 2 is via the definition of the function $\mathbb{P}(u')$, which from (16) is given by

$$\mathbb{P}(u') = \begin{cases} 1/3 & (A, u, v) \in \Theta, \\ n/(n+2) & (A, u, v) \in \mathcal{D} \text{ and } uu' \text{ is a bridge,} \\ 1/(n+2) & (A, u, v) \in \mathcal{D} \text{ and } uu' \text{ is not a bridge.} \end{cases} \quad (18)$$

See Section 2.6 for a discussion of some possible implementations of the required topological queries.

Remark 2.6. The $n \rightarrow 0$ limit of Algorithm 2 is well defined and non-trivial. Taking the $n \rightarrow 0$ limit of (16) or (18) we see that the only change to Algorithm 2 when $n = 0$ is that we are forbidden to delete bridges. If G is hamiltonian, this suggests that the set of recurrent Eulerian states should be the set of all Hamiltonian cycles of G . Indeed, the $n \rightarrow 0$ limit of (17) shows that $\pi_{G,n=0}$ uniformly samples Hamiltonian cycles, and it is supported on the subset of $\mathcal{R}(G)$ in which the spanning subgraphs (V, A) are connected.

While it therefore seems plausible that the $n \rightarrow 0$ limit of Algorithm 2 provides a valid Monte Carlo method for uniformly sampling Hamiltonian cycles, our general proof of the ergodicity of (16) breaks down at $n = 0$. Although Algorithm 2 is very well suited to simulating fully-packed loops for $n > 0$, it is not perhaps the most natural nor the most efficient dynamics for the special case of $n = 0$, and so we have not attempted to prove its ergodicity in this limit. A more natural worm dynamics for simulating Hamiltonian cycles is presented in [48, 49], applying earlier ideas from [50]. We expect the specialized dynamics presented in [48, 49] is more efficient than the $n \rightarrow 0$ limit of Algorithm 2, and it has the added advantage that it simultaneously simulates both Hamiltonian paths and Hamiltonian cycles.

2.5. Ergodicity of $P_{G,n}$

We begin by making some brief comments on our notation. Consider a Markov chain on a state space \mathcal{S} , with transition matrix P . We say $s \in \mathcal{S}$ communicates with $s' \in \mathcal{S}$, and write $s \rightsquigarrow s'$, if the chain may ever visit state s' with positive probability, having started in state s . We say states s and s' intercommunicate, and write $s \leftrightarrow s'$, if $s \rightsquigarrow s'$ and $s' \rightsquigarrow s$. Using this notation, a set of states $\mathcal{A} \subseteq \mathcal{S}$ is ergodic iff $s \leftrightarrow s'$ for all $s, s' \in \mathcal{A}$. Finally, we say P is ergodic if \mathcal{S} is ergodic under P .

Proposition 2.4. *If G is a finite, connected, bipartite cubic graph and $n > 0$, then $P_{G,n}$ is ergodic.*

Proof. Let G be a finite, connected, bipartite cubic graph, let $B \in \mathcal{F}(G)$ be an arbitrary, but fixed, fully-packed subgraph, and let $z \in V$ be an arbitrary, but fixed, vertex. We begin by proving that $(A, u, v) \rightsquigarrow (B, z, z)$ for every $(A, u, v) \in \mathcal{R}(G)$.

Suppose, then, that $(A, u, v) \in \mathcal{R}(G)$. We can generate a new state from (A, u, v) via the map $f : \mathcal{R}(G) \rightarrow \mathcal{R}(G)$ with $f(A, u, v)$ defined by the following prescription:

```

if  $d_u(A) = 1$  then
  Choose an edge  $uu' \in B$  with  $uu' \notin A$ 
  return  $(A \cup uu', u', v)$ 
else if  $d_v(A) = 1$  then
  Choose an edge  $vv' \in B$  with  $vv' \notin A$ 
  return  $(A \cup vv', u, v')$ 
else if  $d_u(A) = 2$  and  $A \neq B$  then
  Choose  $ww' \in B$  with  $ww' \notin A$ 

```

return $(A \cup ww', w', w)$
else if $d_u(A) = 2$ and $A = B$ **then**
return (B, z, z)
else if $d_u(A) = 3$ **then**
Choose the edge $uu' \notin B$
return $(A \setminus uu', u', v)$
end if

The key observation to make is that $(A, u, v) \rightsquigarrow f(A, u, v)$ for every $(A, u, v) \in \mathcal{R}(G)$. Indeed, if $d_u(A) \neq 2$ we simply have $P_{G,n}[(A, u, v) \rightarrow f(A, u, v)] > 0$. Suppose instead that $d_u(A) = 2$, which implies $u = v$. Lemma 2.5 shows that $(A, u, u) \rightsquigarrow (A, w, w)$ for all $u, w \in V$, so if $A = B$ then we clearly have $(A, u, v) = (B, u, u) \rightsquigarrow (B, z, z) = f(A, u, v)$. On the other hand, if $A \neq B$, then there must be at least one edge ww' which is in B but not in A . Again, Lemma 2.5 shows that $(A, u, u) \rightsquigarrow (A, w, w)$, and in addition we have

$$P_{G,n}[(A, w, w) \rightarrow (A \cup ww', w', w)] > 0,$$

so that $(A, w, w) \rightsquigarrow (A \cup ww', w', w)$, and consequently $(A, u, u) \rightsquigarrow (A \cup ww', w', w)$. Therefore, we indeed have $(A, u, v) \rightsquigarrow f(A, u, v)$, and in fact $(A, u, v) \rightsquigarrow f^n(A, u, v)$ for any $n \in \mathbb{N}$, where $f^n = f \circ f \circ \dots \circ f$ denotes n -fold composition of f with itself.

Now, whenever $A \neq B$, the state $f(A, u, v)$ has either one more occupied B -edge, or one less occupied non- B -edge, compared to (A, u, v) . Therefore, since there are only a finite number of edges in G , if we start in any $(A, u, v) \in \mathcal{R}(G)$ and apply f repeatedly, then we must eventually have $f^n(A, u, v) = (B, z, z)$, with n necessarily *finite*. It then immediately follows that $(A, u, v) \rightsquigarrow (B, z, z)$. Finally, the reversibility of $P_{G,n}$ now implies that in fact $(A, u, v) \rightsquigarrow (B, z, z)$, and since this holds for all $(A, u, v) \in \mathcal{R}(G)$ this implies $P_{G,n}$ is ergodic. \square

Lemma 2.5. *Let G be a finite, connected, bipartite cubic graph. For every $A \in \mathcal{F}(G)$ and every pair $x, y \in V$ we have $(A, x, x) \rightsquigarrow (A, y, y)$ under $P_{G,n}$.*

Proof. We begin by showing that $(A, x, x) \rightsquigarrow (A, x', x')$ for all $x \in V$ and $x' \sim x$, where $x' \sim x$ denotes that x' and x are adjacent (i.e. they are neighbors). Firstly, note that if $xx' \notin A$, then we simply have $P_{G,n}[(A, x, x) \rightarrow (A \cup xx', x', x)] > 0$ and $P_{G,n}[(A \cup xx', x', x) \rightarrow (A, x', x')] > 0$, which immediately implies $(A, x, x) \rightsquigarrow (A, x', x')$ in this case.

Therefore, let us consider $x'' \sim x$ with $xx'' \in A$. Lemma 2.6 guarantees that there exists an alternating path, $\mathcal{P} = z_1 z_2 \dots z_{2k}$, such that $z_1 = x$, $z_{2k} = x''$, $z_i z_{i+1} \notin A$ for i odd, and $z_i z_{i+1} \in A$ for i even. The key observation is that it is always possible, via transitions of $P_{G,n}$, to move one defect along such a path while leaving the other defect fixed, which can be seen as follows. Since $(A, z_1, z_1) \in \mathcal{E}$, we can always make the transition $(A, z_1, z_1) \rightarrow (A \cup z_1 z_2, z_2, z_1)$ when $z_1 z_2 \notin A$. Furthermore, since $|A| = |V|$ and $z_3 \neq x$, it follows that $(A \cup z_1 z_2, z_2, z_1) \in \mathcal{D} \cup \Theta$ and $(A \cup z_1 z_2 \setminus z_2 z_3, z_3, z_1) \in \mathcal{T}$. In general, if the position of the first defect is z_i with i even, then the corresponding state will be in $\mathcal{D} \cup \Theta$, and the transition that moves the first defect from z_i to z_{i+1} by deleting the edge $z_i z_{i+1}$ will occur with strictly positive probability. Conversely, if the position of the first defect is z_i with $i > 1$ odd, then the corresponding state will be in \mathcal{T} , and since $z_i z_{i+1} \notin A$, the transition that moves the first defect from z_i to z_{i+1} by adding the edge $z_i z_{i+1}$ will also occur with strictly positive probability. Consequently,

$$(A, z_1, z_1) \rightsquigarrow (A \Delta E(\mathcal{P}), z_{2k}, z_1) \in \mathcal{D} \cup \Theta.$$

Now we can move the second defect along \mathcal{P} , leaving the first defect fixed at z_{2k} . This has the effect of flipping each edge back to its original state, so we arrive at (A, x'', x'') . Indeed, an analogous argument to that above shows that

$$(A\Delta E(\mathcal{P}), z_{2k}, z_1) \rightsquigarrow (A\Delta E(\mathcal{P})\Delta E(\mathcal{P}), z_{2k}, z_{2k}) = (A, x'', x'').$$

Therefore, $(A, x, x) \rightsquigarrow (A, x', x')$ for all $x' \sim x$. However, since this was proved for general x , it follows that precisely the same argument could be applied to show that $(A, x', x') \rightsquigarrow (A, x, x)$, and so we have $(A, x, x) \rightsquigarrow (A, x', x')$. Finally, since G is connected, transitivity immediately implies that in fact $(A, x, x) \rightsquigarrow (A, y, y)$ for every $y \in V$. \square

Remark 2.7. We remark that the dynamics of the worm algorithm along alternating paths discussed in Lemma 2.5, is very similar to the use of alternating paths by graph theorists in the construction of maximal matchings; see e.g. [37].

Lemma 2.6. *Let G be a finite, connected, bipartite cubic graph. For every $A \in \mathcal{F}(G)$, every $x \in V$, and every $x' \sim x$, there exists a path $z_1 z_2 \dots z_{2k}$ in G such that $z_1 = x$, $z_{2k} = x'$, $z_i z_{i+1} \notin A$ for i odd, and $z_i z_{i+1} \in A$ for i even.*

Proof. We begin by noting that any path \mathcal{P} between x and $x' \sim x$ must have odd length, because $\mathcal{P} + xx'$ is a cycle and G is bipartite.

Now, let $A \in \mathcal{F}(G)$ and $x \in V$, and suppose $xx' \notin A$, $xx'', xx''' \in A$. The path xx' is then trivially a path of the above form, with $k = 1$, so let us focus on constructing a path from x to x'' .

Let $z_1 z_2 \dots z_{2k} z_1$ be a cycle in (V, A) . Since it contains an even number of edges, we can colour half of them blue, and half of them red, in such a way that each vertex z_i is incident to precisely one blue edge and one red edge. For example, we can colour each edge $z_i z_{i+1}$ blue if i is even and red if i is odd. In this way the edges alternate red, blue, \dots , red, blue as we traverse the cycle. Since the cycles in (V, A) are vertex disjoint, such colourings can be performed independently for each cycle.

After performing such a colouring, each vertex in (V, A) is incident to precisely one red, one blue, and one vacant edge. If we now colour each vacant edge green, then we obtain a proper 3-edge-colouring of G . Suppose we now interpret the red edges as vacant, and the blue and green edges as occupied. Each vertex will again have degree 2 (one blue edge plus one green edge), so this procedure generates a new bond configuration $A_{\text{red}} \in \mathcal{F}(G)$. Furthermore, since each vertex is incident to precisely one green edge and one blue edge, each cycle $z_1 z_2 \dots z_{2k} z_1$ in A_{red} must be such that the edges alternate green, blue, \dots , green, blue as we traverse the cycle.

Now, fix $A \in \mathcal{F}(G)$ and $x \in V$, and suppose $xx' \notin A$, $xx'', xx''' \in A$. Suppose we perform a colouring of A , as described above, in which the edge xx'' is blue. It then follows that there is a cycle $z_1 z_2 \dots z_{2k} z_1$ in (V, A_{red}) in which $z_1 = x$, $z_2 = x'$ and $z_{2k} = x''$. But this defines a path $z_1 z_2 \dots z_{2k}$ in G in which the edges $z_i z_{i+1}$ are green (vacant in (V, A)) when i is odd, and blue (occupied in (V, A)) when i is even. We have therefore showed that there exists an alternating path of the required form between x and x'' . A similar argument can obviously be used to construct the required path between x and x''' ; in fact the same colouring can be used as for the xx'' path, provided we interpret the red and green edges as occupied, and the blue edges as vacant. \square

2.6. Connectivity-checking and the colouring method

An important practical matter when implementing the algorithms we have presented so far, is the need, when $n \neq 1$, to perform a non-local query to determine if the cyclomatic number changes when an update is performed. Consider a spanning subgraph $(V, A) \subseteq G$ of a graph $G = (V, E)$. Since the number of components, $k(A)$, is related to the cyclomatic number, $c(A)$, by $k(A) = |V| - |A| + c(A)$, the task of determining whether an edge-update changes the cyclomatic number is equivalent to determining whether it changes the number of connected components. The latter question can be answered by known dynamic connectivity-checking algorithms [51], which take polylogarithmic amortized time. A much simpler approach, which runs in polynomial time, but with a (known) small exponent is simultaneous breadth-first search [52]. We used the latter approach in the simulations presented in Section 3. In Sections 2.6.1 and 2.6.2 we discuss a different approach, the *colouring method*, which avoids altogether the need for such global queries, at least when $n > 1$. Before discussing the colouring method, however, we make some remarks regarding the practical implementation of connectivity queries.

To illustrate, we will consider Algorithm 2 with $n > 1$. Algorithm 2 states that connectivity queries are necessary only when $(A, u, v) \in \Theta \cup \mathcal{D}$. In practice, however, even in this case one does not usually need to perform such queries. Suppose we assign a fixed (but arbitrary) ordered labeling to V , so $V = \{v_1, v_2, \dots\}$, and let $r \in [0, 1]$ be a uniformly-distributed random number. For notational convenience we set $p = 1/(n + 2)$ and $\epsilon = 1/3 - p > 0$. We can implement the $d_u(A) = d_v(A) = 3$ block in Algorithm 2 as follows. Denote the neighbors of u by u_j with $j = 1, 2, 3$, such that u_1 has the smallest label, and u_3 the largest. If $r \in [(j - 1)p, jp]$ then we can simply choose u_j without knowing the topology of the defect cluster. If instead $r > 3p$, then we need to determine whether or not any of the edges uu_j are bridges; there can be at most one. If uu_j is a bridge then we choose u_j , otherwise if none of the uu_j are bridges then we choose uu_j iff $r \in [3p + (j - 1)\epsilon, 3p + j\epsilon]$. An analogous trick can be employed when $n < 1$.

The computational burden imposed by these connectivity queries is of greater concern when $x < \infty$ than when $x = \infty$. At $x = +\infty$, connectivity-checking is only required when $d_u(A) = d_v(A) = 3$. By contrast, when $x < \infty$ it is in principle always necessary unless both defects are isolated, except where avoided by a trick of the type described above. For this reason, one might expect that the colouring method (whose raison d'être is to avoid connectivity queries) would be more advantageous when $x < \infty$. Our simulations suggest that this is indeed the case. In fact, while the colouring method was significantly more efficient on the critical branch, it was significantly *less* efficient than the connectivity-checking version when $x = \infty$.

2.6.1. The colouring method

Consider a finite graph $G = (V, E)$. The *colouring method* [16, 18, 24] is a general methodology for simulating models of the form

$$\phi_{G,W}(A) \propto \prod_{C \in K(A)} W(C), \quad A \subseteq E, \quad (19)$$

where $K(A)$ denotes the set of all connected components of (V, A) , and W is an arbitrary map that associates a nonnegative weight to every connected subgraph of G . Many lattice models in statistical mechanics can be expressed in the form (19). If we set $W(C) = q^{|E(C)|}$ for all C , then

we recover the standard random-cluster model of Fortuin-Kasteleyn [19]. If, instead, we set

$$W(C) = \begin{cases} 1, & \text{if } C \text{ is an isolated vertex,} \\ n x^{|E(C)|}, & \text{if } C \text{ is a cycle,} \\ 0, & \text{otherwise,} \end{cases} \quad (20)$$

and G has maximum degree $\Delta(G) \leq 3$, then $\phi_{G,W} = \phi_{G,n,x}$ and we recover the loop model (1).

The key step in applying the colouring method is to choose an appropriate nonnegative weight function $\widehat{W} < W$ for which we have a transition matrix $P_{G,\widehat{W}}$ to simulate $\phi_{G,\widehat{W}}$. In practice, *appropriate* means that $P_{G,\widehat{W}}$ is more efficient/convenient to implement than any algorithm we have at hand for $\phi_{G,W}$. We shall return to this point in Section 2.6.2. Given \widehat{W} and $P_{G,\widehat{W}}$, the colouring method simulates $\phi_{G,W}$ by an algorithm which, at each step, updates the bonds on a suitably-chosen random subgraph $H \subseteq G$ using $P_{H,\widehat{W}}$, while leaving all other bonds fixed.

Algorithm 3 (colouring method).

loop

Current state is $A \subseteq E$

Independently colour each $C \in K(A)$ red with probability $\widehat{W}(C)/W(C)$ and blue otherwise

Identify the active subgraph $G_{\text{red}} = G[V_{\text{red}}]$

Choose a new A'_{red} via $P_{G_{\text{red}},\widehat{W}}[A_{\text{red}} \rightarrow A'_{\text{red}}]$

New state is $A' = A'_{\text{red}} \cup A_{\text{blue}}$

end loop

By independently colouring each cluster in $K(A)$ we obtain a random 2-colouring of the vertices $\sigma \in \{\text{red}, \text{blue}\}^V$ for which each edge in A has both its endpoints coloured the *same* colour. We consider the subgraph induced by the red vertices $G_{\text{red}}(\sigma) = G[V_{\text{red}}(\sigma)]$ as *active* and that induced by the blue vertices as *frozen*. The set $A_{\text{red}} = A \cap E(G_{\text{red}})$ is the subset of all edges in A for which both endpoints lie in V_{red} , and similarly $A_{\text{blue}} = A \cap E(G_{\text{blue}})$.

In Section 2.6.2 we specialize Algorithm 3 to construct a worm algorithm for the loop model $\phi_{G,n,x}$, which we present in Algorithm 4. We conclude the current section by providing a more precise statement of Algorithm 3 in terms of transition matrices. To this end, let us set $\mathbf{W} = (W_{\text{red}}, W_{\text{blue}}) = (\widehat{W}, W - \widehat{W})$ and introduce the following joint measure of colours and bonds

$$\mu_{G,\mathbf{W}}(A, \sigma) \propto \Delta(A, \sigma) \prod_{C \in K(A)} W_{\sigma(C)}(C), \quad (21)$$

where $\sigma(C)$ denotes the colour of the vertices in cluster $C \in K(A)$, and $\Delta(A, \sigma)$ is the indicator for the event $\{(A, \sigma) : \sigma_i = \sigma_j \text{ for all } ij \in A\}$. The transition matrix of the colouring method provides a Monte Carlo algorithm to simulate the joint measure (21). Since the marginal measure $\sum_{\sigma} \mu_{G,\mathbf{W}}(\cdot, \sigma)$ on $\{A \subseteq E\}$ is simply $\phi_{G,W}$, it then follows immediately that the colouring method in fact provides a Monte Carlo method for $\phi_{G,W}$. Proposition 2.7 provides a precise definition as well as a justification of the colouring-method transition matrix. Recall that the support of $\mu_{G,\mathbf{W}}$ is, by definition, $\text{supp}(\mu_{G,\mathbf{W}}) := \{(A, \sigma) : \mu_{G,\mathbf{W}}(A, \sigma) > 0\}$. In a slight abuse of notation, we also write $\sigma \in \text{supp}(\mu_{G,\mathbf{W}})$ whenever there exists $(A, \sigma) \in \text{supp}(\mu_{G,\mathbf{W}})$.

Proposition 2.7 (colouring Method). *Consider $\widehat{W} < W$ with $\text{supp}(\widehat{W}) = \text{supp}(W)$, and for each $\sigma \in \text{supp}(\mu_{G,\mathbf{W}})$ let $P_{G_{\text{red}}(\sigma),\widehat{W}}$ be a transition matrix with state space $\{A_{\text{red}} \subseteq E(G_{\text{red}}(\sigma))\}$*

and stationary distribution $\phi_{G_{\text{red}}(\sigma), \widehat{W}}$, and suppose $P_{G, \widehat{W}}$ is ergodic on $\text{supp}(\phi_{G, \widehat{W}})$. If we define transition matrices P_{colour} and P_{bond} on $\text{supp}(\mu_{G, \mathbf{W}})$ by

$$P_{\text{colour}}[(A, \sigma) \rightarrow (A', \sigma')] = \delta_{A, A'} \Delta(A, \sigma') \prod_{C \in \mathcal{K}(A)} \frac{W_{\sigma'(C)}(C)}{W(C)},$$

$$P_{\text{bond}}[(A, \sigma) \rightarrow (A', \sigma')] = \delta_{\sigma, \sigma'} \Delta(A', \sigma) \delta_{A_{\text{blue}}, A'_{\text{blue}}} P_{G_{\text{red}}(\sigma), \widehat{W}}[A_{\text{red}} \rightarrow A'_{\text{red}}],$$

then $P := P_{\text{colour}} P_{\text{bond}}$ is ergodic and has stationary distribution $\mu_{G, \mathbf{W}}$.

Proof. We simply sketch the proof; see [18, 24] for further details. Ergodicity follows by noting that there is a positive probability of consecutively colouring the whole graph red an arbitrary number of times, and then relying on the ergodicity of $P_{G, \widehat{W}}$. Stationarity of $\mu_{G, \mathbf{W}}$ follows by observing that $\mu_{G, \mathbf{W}}$ is in fact stationary with respect to both P_{colour} and P_{bond} separately, and these latter two facts can be easily verified by noting that $P_{\text{colour}}[(A, \sigma) \rightarrow (A', \sigma')] = \delta_{A, A'} \mu_{G, \mathbf{W}}(\sigma' | A)$, and

$$\mu_{G, \mathbf{W}}(A | \sigma) = \Delta(A, \sigma) \phi_{G_{\text{red}}(\sigma), \widehat{W}}(A_{\text{red}}) \phi_{G_{\text{blue}}(\sigma), \widehat{W}}(A_{\text{blue}}).$$

□

2.6.2. Applying the colouring method to worm algorithms for the loop model

Since we do not need to perform connectivity checks when $n = 1$, we consider worm updates for the $n = 1$ model to be *convenient*, and we know from experience [34, 25] that they are also efficient. When $n > 1$ it is therefore natural to choose

$$\widehat{W}(C) = \begin{cases} x^{|E(C)|}, & \text{if } C \text{ is Eulerian,} \\ 0, & \text{otherwise.} \end{cases} \quad (22)$$

The resulting algorithm proceeds as follows:

Algorithm 4 (coloured worm algorithm).

loop

Current state is A

Colour each isolated vertex red

Independently colour each loop red with probability $1/n$

Identify G_{red}

Choose, uniformly at random, $v \in V(G_{\text{red}})$

Use $n = 1$ worm updates on G_{red} to make a transition $(A_{\text{red}}, v, v) \rightarrow (A'_{\text{red}}, v', v')$

New state is $A' = A'_{\text{red}} \cup A_{\text{blue}}$

end loop

Finally, let us consider the $n = 1$ worm updates in a little more detail. Let $H \subseteq G$ and consider the following transition matrix on $\mathcal{C}(H)$

$$\widetilde{P}_{H, x}[A \rightarrow A'] := \frac{1}{V} \sum_{v, v' \in V} \overline{P}_{H, n=1, x}[(A, v, v) \rightarrow (A', v', v')], \quad (23)$$

where $\overline{P}_{G, n, x}$ is the restriction of (9) to the Eulerian subspace (10). $\widetilde{P}_{H, x}[A \rightarrow A']$ is the probability that, starting in $A \in \mathcal{C}(H)$, we pick, uniformly at random, a location for the defects, v , then

perform worm updates from (A, v, v) until we arrive at a new $A' \in C(H)$, regardless of the new location of the defects. It is clear that the row sums of $\widetilde{P}_{H,x}$ are correctly normalized, so that it defines a stochastic matrix, and it is also clear that $\widetilde{P}_{H,x}$ is in detailed balance with $\phi_{H,n=1,x}$. In addition, since $\widetilde{P}_{G,n,x}$ is ergodic on any G when $x < \infty$, it follows immediately that $\widetilde{P}_{H,x}$ is ergodic for all $x < \infty$. The transition matrices $P_{G_{\text{red}}(\sigma), \widehat{W}}$ required in Proposition 2.7 are then chosen to be $\widetilde{P}_{G_{\text{red}}(\sigma), x}$. Analogous transition matrices can obviously be constructed from (11) and (16). For the fully-packed case, $\widetilde{P}_{H,x=+\infty}$ is not necessarily ergodic on all possible subgraphs, however Proposition 2.7 only requires that it be ergodic for $H = G$, which is guaranteed by Proposition 2.4.

Remark 2.8. Let us return to the case of the genuinely n -dependent connectivity-checking versions of the worm dynamics, as discussed in Sections 2.1, 2.3, and 2.4. We note that the right-hand side of (23), with n left arbitrary rather than fixed to 1, defines a perfectly valid alternative worm algorithm, in which an additional step is added: whenever the defects collide, uniformly at random choose a new vertex to move them both to. In particular, for the FPL model, if one were to add such a move then ergodicity could be proved without recourse to Lemmas 2.5 and 2.6. However, we find empirically that there is no practical advantage to adding these moves, and we did not use them in our simulations (except, of course, when using the colouring method).

3. Numerical results

We simulated the loop model (1) on an $L \times L$ honeycomb lattice with periodic boundary conditions, using the algorithms described in Section 2. In particular, we used the genuinely n -dependent algorithms described in Sections 2.3 and 2.4, as well as the colouring algorithms described in Section 2.6.2. We shall refer to these two distinct versions as the *connectivity-checking* and *colouring* versions, respectively.

We considered both the cases $n \leq 2$ and $n > 2$. The questions studied differed substantially in these two cases, since the exact phase diagram is known when $n \leq 2$, while no exact results are known at all for $n > 2$. For each choice of n , and each possible branch (when $n \leq 2$) we simulated at least seven (and up to eleven) different choices L , in the range $12 \leq L \leq L_{\text{max}}$. The values of L_{max} used depended on the choices of x and n . They are summarized in Table 1.

Table 1: Summary of different values of L_{max} used in each simulation.

	Critical				Densely-packed			Fully-packed						$n > 2$	
n	0.5	1.0	1.5	2.0	0.5	1.0	1.5	0.1	1.0	1.25	1.5	1.75	2.0	3	10
L_{max}	240	360	240	240	120	240	240	120	240	240	240	240	240	120	120

For $n > 2$, we simulated at $n = 3$ and 10, with the aim of verifying the existence of a phase transition, the nature of its universality class, and obtaining accurate estimates of the critical points. For $n \leq 2$, we simulated on both branches of (4), as well as at $x = +\infty$. We focused on identifying the scaling exponents of five distinct classes of observables, characterizing loop lengths, face sizes, the magnetization of dual Ising spin configurations and its staggered analogue, and the return time to the Eulerian subspace. Although the latter observable is, by construction, defined on the full worm space $\mathcal{S}(G)$, rather than on the loop state space $\mathcal{C}(G)$, we shall see that it appears to have a deep connection with the loop model itself.

3.1. Observables measured

We measured the following observables in our simulations. All observables were measured only when the defects coincided, with the exception of the return time, \mathcal{T} , which is defined on the full worm chain.

- The number of loops $\mathcal{N}_l(A) = c(A)$.
- The number of bonds $\mathcal{N}_b(A) = |A|$.

Note that on the fully-packed branch we trivially have $\mathcal{N}_b = |V| = 2L^2$, so we only measured this quantity on the critical and densely-packed branches.

- The length of the largest loop \mathcal{L}_1
- The mean-square loop length

$$\mathcal{L}_2 := L^{-2} \sum_l |l|^2 \quad (24)$$

where the sum is over all loops l .

- The size of the largest face \mathcal{G}_1
- The mean-square face size

$$\mathcal{G}_2 := L^{-2} \sum_f |f|^2 \quad (25)$$

where the sum is over all faces f . Every loop configuration A on the honeycomb lattice can be decomposed into a number of faces, each consisting of a collection of elementary hexagons, such that every pair of neighboring elementary hexagons which share an unoccupied edge in A belong to the same face. The size $|f|$ of face f is then simply the number of elementary hexagons which it contains.

- The dual Ising magnetization \mathcal{M} .

This is measured by assigning an Ising configuration to the dual triangular lattice in such a way that the loops on the honeycomb lattice form the domain boundaries of the Ising spin configuration. Such Ising configurations can be defined in an unambiguous manner whenever the loop configuration winds the torus an even number of times, and we therefore only measured this observable when the loop configuration was in this subspace of the cycle space. In such cases the spin configuration is unique (up to a global spin flip $\sigma \mapsto -\sigma$).

- The sublattice dual Ising magnetization \mathcal{M}_i , for $i = 1, 2, 3$.

Since the triangular lattice is tripartite, we can independently consider the Ising magnetization on each of its three sublattices.

- The return time \mathcal{T} to the Eulerian subspace $C(G) \times V$.

From these observables we estimated the following quantities:

- The loop-number density $n_l := L^{-2} \langle \mathcal{N}_l \rangle$

- The loop-number fluctuation $C_l := L^{-2} \text{var}(\mathcal{N}_l)$
- The bond-number density on the critical and densely-packed branches $n_b := L^{-2} \langle \mathcal{N}_b \rangle$
- The bond-number fluctuation on the critical and densely-packed branches $C_b := L^{-2} \text{var}(\mathcal{N}_b)$
- The expectations $\langle \mathcal{L}_1 \rangle$ and $\langle \mathcal{L}_2 \rangle$
- The expectations $\langle \mathcal{G}_1 \rangle$ and $\langle \mathcal{G}_2 \rangle$
- The dual Ising susceptibility $\chi_{\text{Ising}} = L^{-2} \langle \mathcal{M}_{\text{Ising}}^2 \rangle$
- The second and fourth moments, $\langle \mathcal{M}_{\text{stag}}^2 \rangle$ and $\langle \mathcal{M}_{\text{stag}}^4 \rangle$, of the the staggered dual Ising magnetization, $\mathcal{M}_{\text{stag}}$, defined by

$$\mathcal{M}_{\text{stag}}^2 := (\mathcal{M}_1 - \mathcal{M}_2)^2 + (\mathcal{M}_2 - \mathcal{M}_3)^2 + (\mathcal{M}_3 - \mathcal{M}_1)^2$$

- The staggered susceptibility $\chi_{\text{stag}} = L^{-2} \langle \mathcal{M}_{\text{stag}}^2 \rangle$
- The dimensionless ratio

$$Q_s = \frac{\langle \mathcal{M}_{\text{stag}}^2 \rangle^2}{\langle \mathcal{M}_{\text{stag}}^4 \rangle}$$

- The mean return time to the Eulerian subspace $\langle \mathcal{T} \rangle$. We also estimated the higher-order moments $\langle \mathcal{T}^k \rangle$, for $k = 2, 3, 4$, and the distribution $\mathbb{P}(\mathcal{T} = t)$.

For each quantity $Y = n_l, n_b, C_l, C_b, \langle \mathcal{L}_1 \rangle, \langle \mathcal{L}_2 \rangle, \langle \mathcal{G}_1 \rangle, \langle \mathcal{G}_2 \rangle, \chi_{\text{Ising}}, \chi_{\text{stag}}, Q_s$ and $\langle \mathcal{T}^k \rangle$ we performed a least-squares fit of our Monte Carlo data to the finite-size scaling (FSS) ansatz

$$Y(\beta, L) = c_0 + c_1(\beta - \beta_c) + \dots + L^{x_Y} [a_0 + a_1(\beta - \beta_c)L^{y_i} + a_2(\beta - \beta_c)^2 L^{2y_i} + \dots + b_1 L^{-\omega_1} + b_2 L^{-\omega_2} + \dots] \quad (26)$$

Here y_i is the leading thermal exponent. The a_i are coefficients of the FSS variable $(\beta - \beta_c)L^{y_i}$, the b_i are the coefficients of the corrections-to-scaling terms, and the c_i are the coefficients of analytic terms. There are also cross-terms involving products of terms arising from each of these three sources. The choice of which terms to include in the fit for a given choice of observable varied from case to case, and involved a certain amount of trial and error. The exponent x_Y in (26) is a generic label for whatever the dominant exponent happens to be for the quantity Y . In particular, if Y happens to be dimensionless, such as Q_s , then we have $x_Y = 0$ identically, and in this case all the c_i are identically zero.

As a precaution against corrections to scaling, we imposed a lower cutoff $L \geq L_{\text{min}}$ on the data points admitted to the fit, and we studied systematically the effects on the fit of varying the value of L_{min} . We used the Levenberg-Marquardt algorithm to perform the fits.

3.2. Fits for $n \leq 2$

The results of the fits for $n \leq 2$ are presented in Tables 2, 3 and 4. We discuss these results observable by observable in the following sections.

Table 2: Critical exponents for the critical branch. The exponent X_{worm} denotes the scaling dimension of $\langle \mathcal{T} \rangle$ for the connectivity-checking version of the worm dynamics.

n	X_{loop}	X_{hull}	X_{face}	X_{P_h}	X_{Ising}	X_{P_t}	X_{energy}	X_{stag}	$X_{P_{t2}}$	X_{worm}	X_h
0.5	0.648(2)	0.6478	0.0258(4)	0.0261	0.0567(2)	0.0567	0.816(3)	0.79(2)	0.8178	0.1157(3)	0.1154
1.0	0.623(2)	0.6250	0.0518(4)	0.0521	0.1251(2)	0.1250	0.998(3)	0.97(2)	1.0000	0.1250(2)	0.1250
1.5	0.592(2)	0.5935	0.0800(4)	0.0801	0.2194(2)	0.2195	1.254(5)	1.28(6)	1.2519	0.1322(2)	0.1322
2.0	0.5000(2)	0.5000	0.1249(3)	0.1250	0.4998(3)	0.5000	1.996(7)	–	2.0000	0.1251(5)	0.1250

Table 3: Critical exponents for the densely-packed loop branch. The exponent X_{worm} denotes the scaling dimension of $\langle \mathcal{T} \rangle$ for the connectivity-checking version of the worm dynamics. No exponents are reported for X_{stag} since it was found to be constant.

n	X_{loop}	X_{hull}	X_{face}	X_{P_h}	X_{Ising}	X_{P_t}	X_{worm}	X_h
0.5	0.139(2)	0.1386	0.0640(4)	0.0637	1.58(1)	1.5843	-0.0788(4)	-0.0791
1.0	0.2500(1)	0.2500	0.1044(4)	0.1042	–	–	0.0000(1)	0.0000
1.5	0.3508(3)	0.3506	0.1282(3)	0.1280	0.947(3)	0.9482	0.0620(3)	0.0619

3.2.1. Scaling of energy-like quantities

Standard finite-size scaling arguments predict that on the critical branch

$$n_b \sim a + b L^{y_{\text{energy}} - 2}, \quad (27)$$

$$C_b \sim a + b L^{2y_{\text{energy}} - 2}, \quad (28)$$

where $y_{\text{energy}} = 2 - X_{\text{energy}}$ is the fractal dimension characterizing the energy-like quantities, and X_{energy} is the corresponding scaling dimension. It was observed in [24] that for the critical loop model with $1 < n < 2$, we have $X_{\text{energy}} = X_{P_{t2}}$ where $X_{P_{t2}}$ is the second thermal scaling dimension of the q -state Potts model with $q = n^2$, whose expression in terms of the Coulomb gas coupling g is known [26] to be

$$X_{P_{t2}} = -2 + 16/g. \quad (29)$$

For $n = 1$, one has $X_{P_{t2}} = 1$ and $2y_{\text{energy}} - 2 = 0$, and Eq. (28) is replaced by $C_b \sim a + b \ln L$. Table 2 shows the numerical results, which confirms Eq. (29).

The behaviour of the loop-number density n_l and its fluctuation C_l is also described by Eqs. (27) and (28). This is perhaps unsurprising in light of the Euler relation $c(A) = |A| - |V| + k(A)$.

On any graph of maximum degree 3, the observable $\mathcal{N}_b/\mathcal{N}_l$ is simply the arithmetic mean of the loop lengths in a given configuration. This quantity was studied in detail in [53], and in particular it was found that its expectation $\langle \mathcal{N}_b/\mathcal{N}_l \rangle$ tends to a constant in the thermodynamic limit.

Table 4: Critical exponents on the fully-packed branch. The exponent X_{worm} denotes the scaling dimension of $\langle \mathcal{T} \rangle$ for the connectivity-checking version of the worm dynamics.

n	X_{loop}	X_{hull}	X_{face}	X_{P_h}	X_{Ising}	X_{P_t}	X_{stag}	$2/3g$	X_{worm}	X_h
0.1	0.031(3)	0.0309	0.0154(4)	0.0152	1.92(6)	1.9074	0.322(5)	0.3231	0.032(4)	0.0309
1.0	0.2500(2)	0.2500	0.1042(3)	0.1042	–	1.2500	0.2499(1)	0.2500	0.2498(4)	0.2500
1.25	0.3005(2)	0.3006	0.1181(2)	0.1180	1.10(3)	1.0982	0.2333(3)	0.2331	0.3005(3)	0.3006
1.5	0.3505(4)	0.3506	0.1276(4)	0.1280	0.93(2)	0.9482	0.2165(3)	0.2165	0.3507(3)	0.3506
1.75	0.4039(3)	0.4042	0.1336(3)	0.1335	0.79(1)	0.7875	0.1986(4)	0.1986	0.4043(5)	0.4042
2.0	0.482(3)	0.5000	0.1345(3)	0.1250	0.57(2)	0.5000	0.175(3)	0.1667	0.480(3)	0.5000

On the critical branch, the fitting results for the constants, n_{b0} , C_{b0} , n_{l0} , C_{l0} , and $B = n n_{b0}/n_{l0}$, are shown in Table 5. Our estimate $B(n = 2) = 38.832(2)$ agrees well with $38.834(2)$ in Ref. [53].

On the densely-packed branch, our data indicate that the scaling of n_l and C_l fits well the formula $n_l \sim a + bL^{-2}$ and $C_l \sim a + bL^{-2}$, while for n_b and C_b , there's no detectable finite-size dependence. The asymptotic behaviour of B for $n \rightarrow 0$ agrees with the prediction $B(n \rightarrow 0) = 35.70(2)$ [53].

On the fully-packed branch, we have $N_b = |V|$ and so the expectation of the arithmetic mean of the loop lengths is simply $2/n_l$. Our data for n_l fit the formula $n_l \sim a + bL^{-2}$, however, for $n = 2$ the dominant correction exponent appears to be $-2.20(4)$, most probably arising from logarithmic corrections. No detectable finite-size dependence is found for C_l . For $n = 2$, the estimates for n_{l0} , C_{l0} and B confirm the prediction $n_l = 1/9$, $C_l = 1/9 + 1/135$, and $B = 36$. We also determined the asymptotic value $B(n \rightarrow 0) = 30.04(2)$, in good agreement with the exact value $30.0344\dots$

Table 5: Numerically determined results n_{b0} , C_{b0} , n_{l0} , C_{l0} , and $B = n n_{b0}/n_{l0}$.

Branch	n	n_{b0}	C_{b0}	n_{l0}	C_{l0}	B
Critical	0.5	0.26646(6)	-2.37(4)	0.018644(5)	0.011(4)	7.146(4)
	1.0	0.49998(2)	0.41(4)	0.033664(4)	-0.0072(3)	14.852(3)
	1.5	0.72953(1)	4.8(1)	0.046243(3)	0.078(2)	23.664(3)
	2.0	1.114837(3)	1.789(2)	0.057418(2)	0.0553(2)	38.832(2)
DPL	1.5	1.395506(2)	0.9760(3)	0.0475624(4)	0.03978(2)	44.0108(6)
	1.0	1.499999(2)	0.7500(1)	0.0352504(4)	0.02999(2)	42.5527(6)
	0.5	1.579679(2)	0.5960(2)	0.0199245(6)	0.01798(2)	39.642(2)
FPL	0.1	2	0	0.006527(4)	0.00640(2)	30.642(9)
	1.0	2	0	0.057668(2)	0.05242(3)	34.6813(4)
	1.25	2	0	0.070680(1)	0.06484(4)	35.3707(2)
	1.5	2	0	0.083677(2)	0.07851(5)	35.8521(4)
	1.75	2	0	0.096989(2)	0.0952(2)	36.0866(4)
	2.0	2	0	0.111111(2)	0.1185(1)	36.0000(3)

3.2.2. Scaling of $\langle \mathcal{L}_1 \rangle$ and $\langle \mathcal{L}_2 \rangle$

Standard finite-size scaling arguments predict that

$$\langle \mathcal{L}_1 \rangle \sim L^{y_{\text{loop}}} \quad (30)$$

$$\langle \mathcal{L}_2 \rangle \sim L^{2y_{\text{loop}}-2} \quad (31)$$

where $y_{\text{loop}} = 2 - X_{\text{loop}}$ is the fractal dimension characterizing loop length, and X_{loop} is the corresponding scaling dimension. It was argued in [54] that for the critical loop model we have $X_{\text{loop}} = X_{\text{hull}}$, where X_{hull} is the hull scaling dimension

$$X_{\text{hull}} = 1 - \frac{2}{g}, \quad (32)$$

and g is related to x and n as in (5) and (6). It was argued in [46] that $X_{\text{loop}} = X_{\text{hull}}$ also holds on the fully-packed branch.

On the critical branch, $X_{\text{loop}} = X_{\text{hull}}$ was verified for $1 \leq n \leq 2$ in the Monte Carlo study presented in [24]. Table 2 confirms this result, and shows that it extends to $n < 1$. Since the expression (32) for $X_{\text{hull}}(g)$ as a function of g should be universal, we expect that if we insert the

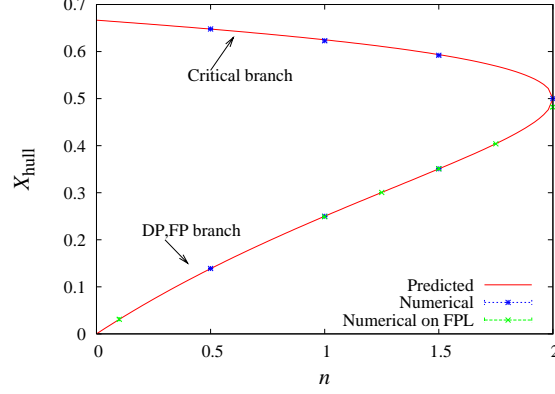


Figure 3: Numerically determined scaling dimension X_{loop} plotted with the exact expression (32) for X_{hull} , as a function of n .

DPL expression for g into (32) then we would again have $X_{\text{loop}} = X_{\text{hull}}$. Table 3 shows that this is indeed the case, and Table 4 shows that the result also holds on the fully-packed branch. In Fig. 3 we plot our numerical estimates of X_{loop} together with the exact result for X_{hull} for all three branches. The agreement is clearly excellent. The small deviation of the FPL estimate at $n = 2$ is presumably due to the presence of logarithmic corrections to scaling.

3.2.3. Scaling of $\langle \mathcal{G}_1 \rangle$ and $\langle \mathcal{G}_2 \rangle$

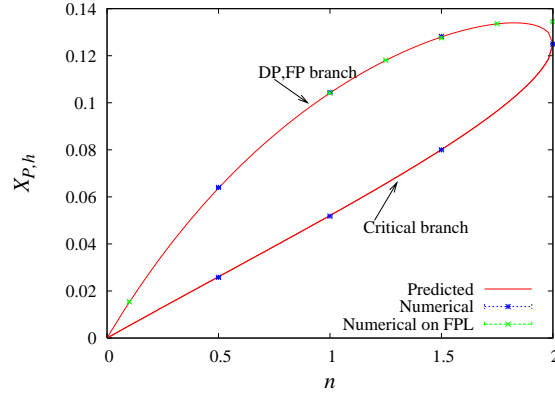


Figure 4: Numerically determined scaling dimension X_{face} plotted with the exact expression (35) for $X_{P,h}$, as a function of n .

Analogously to the previous case for loop length, we expect that

$$\langle \mathcal{G}_1 \rangle \sim L^{y_{\text{face}}} \quad (33)$$

$$\langle \mathcal{G}_2 \rangle \sim L^{2y_{\text{face}}-2} \quad (34)$$

where $y_{\text{face}} = 2 - X_{\text{face}}$ is the fractal dimension characterizing face size, and X_{face} is the corresponding scaling dimension. It was argued in [55] that for both the critical and densely-packed loop models we have $X_{\text{face}} = X_{P,h}$, where $X_{P,h}$ is the magnetic scaling dimension of the q -state Potts model with $q = n^2$, whose expression in terms of the Coulomb gas coupling g is known [26] to be

$$X_{P,h} = \frac{(6-g)(g-2)}{8g}, \quad (35)$$

and g is related to x and n as in (5) and (6).

On the critical branch, $X_{\text{face}} = X_{P,h}$ was verified for $1 \leq n \leq 2$ in the Monte Carlo study presented in [24]. Table 2 confirms this result, and shows that it extends to $n < 1$, and Table 3 verifies it in the densely-packed phase. It is not clear *a priori* that this relationship should also hold in the fully-packed branch, but Table 4 shows that it does. In Fig. 4 we plot our numerical estimates of X_{face} together with the exact result for $X_{P,h}$ for all three branches. The agreement is clearly excellent. The deviation of the FPL estimate at $n = 2$ is presumably due to the presence of logarithmic corrections-to-scaling.

3.2.4. Scaling of χ_{Ising}

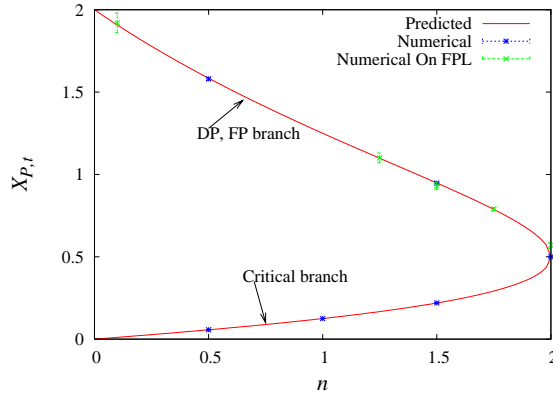


Figure 5: Numerically determined scaling dimension X_{Ising} plotted with the exact expression (37) for $X_{P,t}$, as a function of n .

It is natural to expect that

$$\chi_{\text{Ising}} \sim L^{2-2X_{\text{Ising}}} \quad (36)$$

for some scaling dimension X_{Ising} . It is not *a priori* obvious what the form of X_{Ising} should be, however it was observed in [24] for $1 \leq n \leq 2$ that on the critical branch we have $X_{\text{Ising}} = X_{P,t}$, where $X_{P,t}$ is the thermal scaling dimension of the q -state Potts model with $q = n^2$, whose expression in terms of the Coulomb gas coupling g is known [26] to be

$$X_{P,t} = \frac{6}{g} - 1, \quad (37)$$

and where $g \in [4, 6]$ is related to x and n as in (5). Table 2 confirms this result, and shows that it extends to $n < 1$. One would expect that the relationship would continue into the densely-packed phase, with $g \in [2, 4]$, and Table 3 shows that this is indeed the case. It is not entirely

obvious what the behaviour should be on the fully-packed branch, but Table 4 shows that it simply coincides with that of the densely-packed branch. We note that on the densely-packed and fully-packed branches, when $x < \sqrt{2}$ we have $2 - 2X_{\text{Ising}} < 0$ and so in these cases we estimated X_{Ising} from an ansatz of the form

$$\chi_{\text{Ising}} = a + bL^{2-2X_{\text{Ising}}} + \dots \quad (38)$$

in which the $L^{2-2X_{\text{Ising}}}$ term is sub-dominant.

In Fig. 5 we plot our numerical estimates of X_{Ising} together with the exact result for $X_{P,t}$ for all three branches. The agreement is clearly excellent. We note that there is no data point for $n = 1$ on the densely-packed branch, since $(x, n) = (1, 1)$ simply corresponds to site percolation on the dual triangular lattice (the $+$ ($-$) spins are regarded as occupied (vacant) sites). In this case, the nontrivial dependence of χ_{Ising} on the system size vanishes; i.e. the amplitude a_0 in (26) is identically zero.

3.2.5. Scaling of χ_{stag}

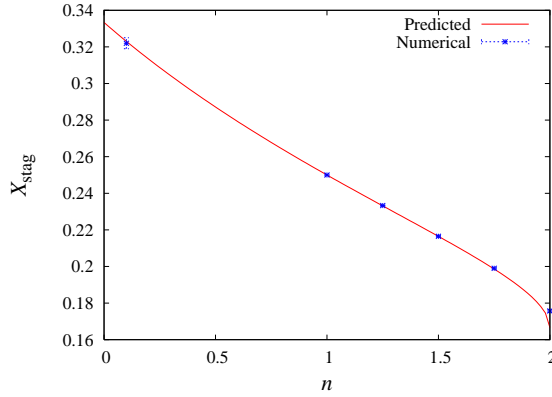


Figure 6: Numerically determined scaling dimension X_{stag} as a function of n in the fully-packed phase, plotted with the conjectured exact expression $X_{\text{stag}} = 2/3g$.

On the critical branch, one might intuitively expect that χ_{stag} converges to a constant as L increases, since the symmetry of the sublattices should cause the staggered magnetization to cancel out for ferromagnetic models. Indeed, our numerical data show that on the critical branch χ_{stag} is well described by the simple FSS ansatz

$$\chi_{\text{stag}} = a + bL^{-X_{\text{stag}}}. \quad (39)$$

Perhaps surprisingly, our data also strongly suggest that we can in fact make the identification $X_{\text{stag}} = X_{P,t2}$ where $X_{P,t2}$ is the second thermal scaling dimension of the q -state Potts model with $q = n^2$, whose expression in terms of the Coulomb gas coupling g is (29). See Table 2.

In the densely-packed phase, when $n = 1$ it is clear that χ_{stag} is simply a constant which displays no finite-size dependence, since the model corresponds to site percolation on the triangular lattice in this case. It is not obvious that this behaviour should persist when $n \neq 1$, however

our simulations strongly suggest that this is indeed the case: we find empirically that there is no finite-size dependence of χ_{stag} for any $0 < n \leq 2$ on the densely-packed branch.

In the fully-packed phase, the $n = 1$ case corresponds to the zero-temperature antiferromagnetic Ising model on the dual triangular lattice, which is known to be critical, and χ_{stag} is its order parameter. It follows that for $n = 1$ we have

$$\chi_{\text{stag}} \sim L^{2-2X_{\text{stag}}} \quad (40)$$

with $X_{\text{stag}} = 1/4$. Our numerical results show convincingly that in fact (40) holds for all $n \leq 2$. However, we were not able to identify the exponent X_{stag} in terms of other known exponents. Instead, we fitted our empirical estimates of X_{stag} to a simple Coulomb-gas ansatz

$$X(g) = \frac{ag^2 + bg + c}{dg} \quad (41)$$

with a, b, c, d unknown integers. We found that X_{stag} is well described by the simple formula (see Fig. 6)

$$X_{\text{stag}} = \frac{2}{3g}. \quad (42)$$

Based on the agreement presented in Table 3, we conjecture that this formula is in fact exact.

3.2.6. Scaling of $\langle \mathcal{T} \rangle$

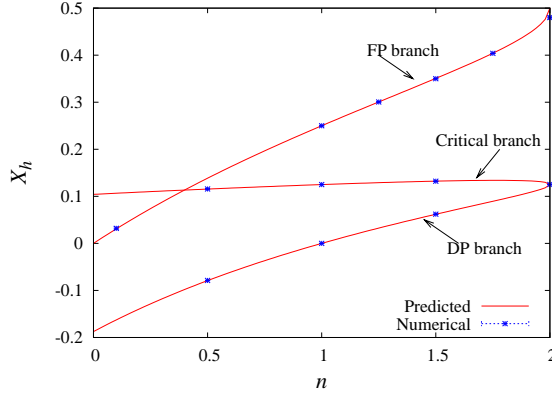


Figure 7: Numerically determined scaling dimension X_{worm} plotted with the exact prediction for X_h as a function of n .

It is natural to expect that

$$\langle \mathcal{T} \rangle \sim L^{2y_{\text{worm}}-2} \quad (43)$$

where $y_{\text{worm}} = 2 - X_{\text{worm}}$ is a fractal dimension characterizing the time of return to the Eulerian subspace $\mathcal{C}(G) \times V \subseteq \mathcal{S}(G)$ in the connectivity-checking version of the worm dynamics.

Although \mathcal{T} is inherently an observable on the state space of the worm dynamics, $\mathcal{S}(G)$, rather than on the state space of the loop model, $\mathcal{C}(G)$, its scaling is linked to the loop model in a fundamental way. In fact, we find numerically that $X_{\text{worm}} = X_h$ for all three branches and for all $n \leq 2$, where X_h is the magnetic scaling dimension of the $O(n)$ loop model. We note that, as

shown in [33, 34], on the critical branch of the $n = 1$ model $\langle \mathcal{T} \rangle$ is equal to the susceptibility of the Ising model whose high-temperature graphs are sampled by the worm dynamics. Therefore, in this special case we have a sound theoretical argument that $X_{\text{worm}} = X_h$, so the general result is not completely unexpected.

On the critical and densely-packed branches, the exact expression [43, 41] for X_h is given by

$$X_h = 1 - \frac{2}{g} - \frac{3}{32}g, \quad (44)$$

where g is related to x and n as in (5) and (6), while on the fully-packed branch it is [44, 45, 46]

$$X_h = 1 - \frac{2}{g}, \quad (45)$$

with $g \in [2, 4]$ related to n as in (5). Tables 2, 3 and 4 show a comparison between X_{worm} and X_h , and in Fig. 7 we plot our numerical estimates of X_{worm} together with the exact result for X_h for all three branches. The agreement is clearly excellent.

Based on these results for the honeycomb lattice, it appears that the identity $X_{\text{worm}} = X_h$ is a generic property of the worm algorithms we present. Preliminary results for the hydrogen-peroxide lattice further support this conjecture; these results will be reported in detail elsewhere. For this reason, it seems in a certain sense that the worm algorithm provides the *natural* dynamics for the $O(n)$ loop model. The relation $X_{\text{worm}} = X_h$ also has some important practical consequences, since it provides a simple way of directly measuring X_h . As one application, it can be used to obtain an accurate estimate of the curve $X_h(n)$ as a continuous function of n in three dimensions, where no exact results are currently known.

The identification $X_{\text{worm}} = X_h$ also has implications for the efficiency of the worm dynamics. For $n < 1$, the exponent $2 - 2X_h$ governing $\langle \mathcal{T} \rangle$ is greater than 2 in the densely-packed phase, implying that it takes a time larger than order volume between visits to the Eulerian subspace. The efficiency of the worm dynamics will therefore suffer in this region. By contrast, on the critical branch one has $2 - 2X_h \in (1.73, 1.8)$ for all $0 \leq n \leq 2$, while on the fully-packed branch $2 - 2X_h$ decreases monotonically with $n \in [0, 2]$ from 2 to 1.

Remark 3.1. Although we have not proved that Algorithm 2 remains ergodic at $n = 0$, we used it to perform simulations of the uniform Hamiltonian cycle model, and we found that $X_{\text{worm}} = 0 = X_h(n = 0)$. This provides some modest evidence that the conjecture $X_{\text{worm}} = X_h$ in fact extends to $n = 0$ when $x = \infty$, and also that Algorithm 2 may indeed be ergodic.

Remark 3.2. For both the critical branch and densely-packed branch, one has the choice of using either the simple worm dynamics, given by (9), or the rejection-free worm dynamics (11). Perhaps unsurprisingly, both versions have the same value of X_{worm} . On the fully-packed branch, only the rejection-free dynamics can be used, since the simple dynamics is non-ergodic.

Remark 3.3. When $n > 1$, one can also consider X_{worm} for the colouring version of the worm dynamics. On the critical branch, we simulated both versions and measured \mathcal{T} in both cases. There appears to be no reason, *a priori*, for $\langle \mathcal{T} \rangle$ in the two cases to be related in any simple way, or even to share the same value of X_{worm} . However, empirically, we found that on the critical branch the exponent X_{worm} governing $\langle \mathcal{T} \rangle$ agrees, within error bars, for the two versions. On the densely-packed branch, by contrast, we found $X_{\text{worm}} = 0.053(2)$ for the colouring version when $n = 1.5$, which appears to disagree with the value $X_{\text{worm}} = 0.0620(3)$ for the connectivity-checking version reported in Table 3. Note that this implies the colouring version has the larger

Table 6: Estimated values of the scaling exponents, y and τ , appearing in the ansatz (46) for the distribution $\mathbb{P}(\mathcal{T} = t)$. Values for the critical, densely-packed, and fully-packed branches are shown.

n	Critical			Densely-packed			Fully-packed		
	τ	y	y_{worm}	τ	y	y_{worm}	τ	y	y_{worm}
0.1	–	–	–	–	–	–	1.166(6)	2.32(1)	1.968(4)
0.5	1.286(4)	2.479(4)	1.8843(3)	1.044(5)	2.257(7)	2.0788(4)	–	–	–
1	1.248(3)	2.325(3)	1.8750(2)	1.077(4)	2.164(6)	2.0000(1)	1.364(3)	2.360(5)	1.7502(4)
1.5	1.223(4)	2.234(4)	1.8678(2)	1.108(5)	2.103(8)	1.9380(3)	1.471(4)	2.458(7)	1.6493(3)
2	1.174(4)	2.120(4)	1.8749(5)	–	–	–	1.602(5)	2.62(1)	1.520(3)

mean return time $\langle \mathcal{T} \rangle$, since $2 - 2X_{\text{worm}}$ is larger in this case. Since we only simulated one value of $n > 1$ on the DP branch, this is the only point where a comparison between the two versions can be made. We did not perform any systematic numerical tests of the colouring algorithm in the fully-packed phase, since our preliminary results suggested it was significantly less efficient than the connectivity-checking version.

3.2.7. Scaling of $\mathbb{P}(\mathcal{T} = t)$

In order to better understand the behaviour of \mathcal{T} , we computed its histogram and thereby estimated its distribution $\mathbb{P}(\mathcal{T} = t)$. One expects that $\mathbb{P}(\mathcal{T} = t)$ obeys a scaling law for large t in a critical system. More precisely, we expect that at finite volume we have

$$\mathbb{P}(\mathcal{T} = t) \sim t^{-\tau} f(t/L^y), \quad (46)$$

for some choice of exponents τ and y , and some scaling function f . Note that the ansatz (46) implies that $\langle \mathcal{T}^k \rangle \sim L^{(k+1-\tau)y}$ to leading order as $L \rightarrow \infty$.

The distribution of the loop length was studied in [46] and found to be of the form (46). We have computed the distributions of \mathcal{L}_2 and \mathcal{G}_2 in the present work, and also found excellent fits to (46). In addition, distributions of the form (46) are known to govern the cluster-size of the random cluster model [52]. For all these cases, the exponent y appearing in (46) coincides with the fractal dimension of the corresponding geometric objects; in particular we have $y = y_{\text{face}} = 2 - X_{P,h}$ and $y = y_{\text{loop}} = 2 - X_{\text{hull}}$ for the face-size and loop-size cases, respectively. In such cases the two parameters y and τ appearing in (46) can be related by the following argument. Consider a generic observable \mathcal{A} characterizing a geometric property (cluster-size, loop-size, face-size...) with fractal dimension $y_{\mathcal{A}}$. Since a given object has scale $L^{y_{\mathcal{A}}}$, the probability of picking one at random should be $\sim L^{y_{\mathcal{A}}}/L^d$ so that we expect $\langle \mathcal{A}^k \rangle \sim L^{y_{\mathcal{A}}-2} L^{ky_{\mathcal{A}}} = L^{(k+1)y_{\mathcal{A}}-2}$. Combining this latter result with the fact that $\langle \mathcal{A}^k \rangle \sim L^{(k+1-\tau)y}$, and assuming $y = y_{\mathcal{A}}$, it follows that $\tau = 2/y$.

Table 6 lists our fits for y and τ , together with y_{worm} for ease of comparison, and Fig. 8 shows a finite-size scaling plot of $\mathbb{P}(\mathcal{T} \geq t)$ for $n = 1$ on the critical branch. Contrary to the observables discussed above, our numerical results show clearly that for the observable \mathcal{T} , the exponent y appearing in (46) is *not* equal to the corresponding fractal dimension y_{worm} . Although the combined exponent $(2 - \tau)y = 2 - 2X_h$ governing the mean $\langle \mathcal{T} \rangle$ is universal, it remains an open question whether or not τ and y are themselves universal. We tried to fit the values of y in Table 6 to the ansatz (41) with $d = 8, 12$, and 16 , but we did not obtain a meaningful expression within the estimated statistical errors.

3.3. $O(n)$ loop model for $n > 2$

Until quite recently, it was generally believed [56] that the (two-dimensional) $O(n)$ loop model, (1), does not exhibit a phase transition when $n > 2$. Using numerical transfer matrix

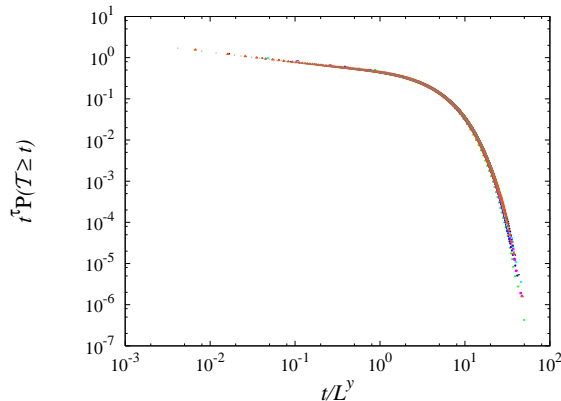


Figure 8: Finite-size-scaling plot showing $t^r \mathbb{P}(\mathcal{T} \geq t)$ versus t/L^y for $n = 1$ on the critical branch, with system sizes $L = 12, 24, 48, 96, 192, 384, 768$.

Table 7: Estimates of X_t , X_h and x_c for the $O(n)$ loop model with $n = 3, 10$. For comparison, note that for the critical 3-state Potts we have $X_t = 4/5$ and $X_h = 2/15$.

n	x_c	X_t	X_h
3	6.822(7)	0.81(3)	0.132(3)
10	1.5430(2)	0.83(4)	0.135(4)

methods, however, strong evidence was found in [21] that a line of critical points does in fact exist for all $n > 2$. Furthermore, the results presented in [21] also suggest that this phase transition falls into the three-state Potts universality class. This can be understood by noting that the $n \rightarrow \infty$ loop model is equivalent to the hard-hexagon model [7].

We performed Monte Carlo simulations of the $n = 3$ and $n = 10$ loop models, using the worm algorithm presented in Section 2. We computed the staggered magnetization on the dual triangular lattice, which allowed us to then compute the staggered susceptibility and the dimensionless ratio Q_s . By studying Q_s we could accurately locate the critical point. See Fig. 9 and Table 7. By studying both χ_{stag} and Q_s we also estimated the exponents X_t and X_h . See Table 7. Our numerical values for X_t and X_h are entirely consistent with a transition in the 3-state Potts universality class, which has $X_t = 4/5 = 0.8000$ and $X_h = 2/15 = 0.1333$.

For comparison, we note that in [21] it was estimated that $x_c = 1.52(1)$, $X_t = 0.80(1)$ and $X_h = 0.14(1)$ for $n = 10$. No data for $n = 3$ was reported in [21], however their quoted values for $n = 4$ were $X_t = 0.76(5)$ and $X_h = 0.1(1)$. A number of different n values were reported in [21], and the accuracy of their estimated exponents was found to increase with n . By contrast, we found the computational effort required for the $n = 3$ and $n = 10$ cases to be comparable.

4. Discussion

We have presented a Markov-chain Monte Carlo algorithm of *worm* type that correctly simulates the $O(n)$ loop model on any bipartite cubic graph, for any $n \in (0, \infty)$ and $x \in (0, \infty]$, and we have proved rigorously that the algorithm is ergodic and has the correct stationary distribution.

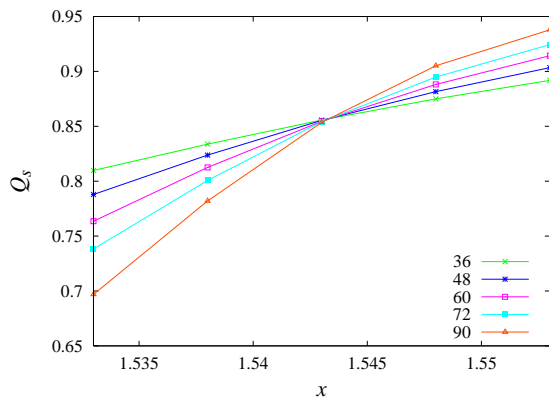


Figure 9: The Binder cumulant Q_s for $n = 10$.

We have then applied this algorithm to the honeycomb-lattice loop model. Comparing our numerical results when $n \leq 2$ with Coulomb gas theory allowed us to identify the exact exponents of a number of fundamental geometric observables, as well as observables related to dual Ising spins. Furthermore, we have provided compelling numerical evidence that $X_{\text{worm}} = X_h$ in all three branches for all $n \leq 2$. This suggests that X_{worm} can be used as an efficient means to estimate X_h in models where no theoretical predictions exist, such as in three dimensions. For the case $n > 2$, we confirmed the existence of a phase transition in the 3-state Potts universality class, which has previously been observed using transfer matrices. Equipped with our worm algorithm, it is now natural to repeat these studies on bipartite cubic graphs other than the honeycomb-lattice, including to the Hydrogen-peroxide lattice, which provides a natural three-dimensional generalization, and the $(4 \cdot 8^2)$ Archimedean lattice, which is the dual of the Union Jack lattice. These results will be reported elsewhere.

Another natural application of the worm algorithms presented in this article is to the study of antiferromagnetic Potts models on triangulations of the torus. Since antiferromagnetic models do not display universality, it is of significant interest to study such models on a variety of different lattices. As discussed in the introduction, it is well known that the honeycomb-lattice FPL model with $n = 1$ is equivalent to the zero-temperature triangular-lattice antiferromagnetic Ising model. While cluster algorithms [27, 28] for this model are thought to be non-ergodic, the worm algorithm presented in Section 2 provides a provably valid Monte Carlo method; see [25].

This observation can be generalized in two ways. Firstly, the dual of any bipartite cubic map on the torus is an Eulerian triangulation, and the worm algorithm from Section 2 can immediately be applied to study Ising models on these triangulations. Secondly, as already mentioned in the Introduction, the honeycomb-lattice FPL model with $n = 2$ is equivalent to the zero-temperature triangular-lattice 4-state Potts antiferromagnet [29], as well as the zero-temperature kagome-lattice 3-state Potts antiferromagnet. As also already mentioned, the Wang-Swendsen-Kotecký [30] (WSK) cluster algorithm, which is undoubtedly the current state-of-the-art for simulating antiferromagnetic Potts models, has recently been proved [31, 32] to be non-ergodic for both of these models. By contrast, the worm algorithms described in Section 2 have been proved to be ergodic, and they can be easily applied to the corresponding loop models, in order to then study these Potts antiferromagnets. To do so, it is sufficient to simply augment the usual worm

steps with an additional step that randomly assigns an alternating colouring (red, blue, red, . . .) to the edges of each cycle. Each cycle can be coloured in precisely two ways. By interpreting the remaining edges as green, this defines a new transition matrix on 3-edge colourings of the honeycomb lattice, given by $2^{-c(A)}P_{G,n=2}[(A, u, v) \rightarrow (A\Delta uu', u', v)]$. Since $P_{G,n}$ is in detailed balance with $\phi_{G,n}(A) \propto n^{c(A)}$, at $n = 2$ this new transition matrix uniformly samples 3-edge colourings. But since the kagome lattice is the medial graph of the honeycomb lattice, it immediately follows that this new transition matrix in fact uniformly samples 3-vertex colourings of the kagome lattice (i.e. simulates the zero-temperature kagome-lattice Potts antiferromagnet). The 4-state model can be treated in a similar way. Finally, we note that these mappings from $n = 2$ loop models to zero-temperature $q = 3$ and $q = 4$ state Potts models hold quite generally. In particular, the 4-state antiferromagnetic Potts model on a variety of two-dimensional triangulations can be studied using such worm algorithms. All of these possibilities we leave for future work.

Acknowledgments

This work was supported in part by the National Nature Science Foundation of China under Grant No. 10975127, the Anhui Provincial Natural Science Foundation under Grant No. 090416224, and the Chinese Academy of Sciences. The authors wish to thank an anonymous referee for some very valuable comments. YD and TMG are indebted to Jan de Gier, Alan Sokal and Jesús Salas for helpful discussions.

References

- [1] R. B. Potts, Some generalized order-disorder transformations, *Proc. Cambridge Philos. Soc.* 48 (1952) 106–109.
- [2] F. Y. Wu, The Potts model, *Rev. Mod. Phys.* 54 (1982) 235–268.
- [3] F. Y. Wu, Potts model of magnetism, *J. Appl. Phys.* 55 (1984) 2421–2425.
- [4] H. E. Stanley, Dependence of critical properties on dimensionality of spins, *Phys. Rev. Lett.* 20 (1968) 589–592.
- [5] A. Pelissetto and E. Vicari, Critical phenomena and renormalization-group theory, *Phys. Rep.* 368 (6) (2002) 549–727.
- [6] C. M. Fortuin and P. W. Kasteleyn, Random-cluster model 1: Introduction and relation to other models, *Physica* 57 (1972) 536–564.
- [7] E. Domany, D. Mukamel, B. Neinhuis and A. Schwimmer, Duality relations and equivalences for models with $O(n)$ and cubic symmetry, *Nucl. Phys. B* 190 (1981) 279–287.
- [8] J. Dubail, J. L. Jacobsen and H. Saleur, Critical exponents of domain walls in the two-dimensional Potts model, *J. Phys. A: Math. Theor.* 43 (2010) 482002.
- [9] P. Di Francesco, P. Mathieu and D. Sénéchal, *Conformal Field Theory*, Springer-Verlag, New York, 1997.
- [10] W. Kager and B. Nienhuis, A Guide to Stochastic Löwner Evolution and Its Applications, *J. Stat. Phys.* 115 (2004) 1149–1229.
- [11] J. Cardy, SLE for theoretical physicists, *Ann. Phys.* 318 (2005) 81–118.
- [12] D. P. Landau and K. Binder, *A guide to Monte Carlo simulations in statistical physics*, Cambridge University Press, Cambridge, 2005.
- [13] A. D. Sokal, Monte Carlo methods in Statistical Mechanics: Foundations and new algorithms, in: C. DeWitt-Morette, P. Cartier, A. Folacci (Eds.), *Functional Integration: Basics and Applications*, Plenum, New York, 1997, pp. 131–192.
- [14] M. Sweeny, Monte Carlo study of weighted percolation clusters relevant to the Potts models, *Phys. Rev. B* 27 (1983) 4445–4455.
- [15] R. H. Swendsen and Jian-Sheng Wang, Nonuniversal critical dynamics in Monte Carlo simulations, *Phys. Rev. Lett.* 58 (1987) 86–88.
- [16] L. Chayes and J. Machta, Graphical representations and cluster algorithms II, *Physica A.* 254 (1998) 477–516.
- [17] Youjin Deng, Timothy M. Garoni and Alan D. Sokal, Critical Speeding-Up in the Local Dynamics of the Random-Cluster Model, *Phys. Rev. Lett.* 98 (2007) 230602.
- [18] Youjin Deng, Timothy M. Garoni, Jonathan Machta, Giovanni Ossola, Marco Polin and Alan D. Sokal, Critical Behavior of the Chayes-Machta-Swendsen-Wang Dynamics, *Phys. Rev. Lett.* 99 (2007) 055701.

- [19] G. R. Grimmett, *The Random-Cluster Model*, Springer, New York, 2006.
- [20] H. W. J. Blöte and B. Nienhuis, The phase-diagram of the $O(n)$ model, *Physica A*. 160 (1989) 121–134.
- [21] W. Guo, H. W. J. Blöte and F. Y. Wu, Phase Transition in the $n > 2$ Honeycomb $O(n)$ Model, *Phys. Rev. Lett.* 85 (2000) 3874–3877.
- [22] M. Karowski, H. J. Thun, W. Helfrich and F. S. Rys, Numerical study of self-avoiding loops on d -dimensional hypercubic lattices, *J. Phys. A: Math. Gen.* 16 (1983) 4073–4081.
- [23] Chengxiang Ding, Youjin Deng, Wenan Guo, Xiaofeng Qian and H. W. J. Blöte, Geometric properties of two-dimensional $O(n)$ loop configurations, *J. Phys. A: Math. Theor.* 40 (2007) 3305–3317.
- [24] Youjin Deng, Timothy M. Garoni, Wenan Guo, Henk W. J. Blöte and Alan D. Sokal, Cluster Simulations of Loop Models on Two-Dimensional Lattices, *Phys. Rev. Lett.* 98 (2007) 120601.
- [25] Wei Zhang, T. M. Garoni and Youjin Deng, A worm algorithm for the fully-packed loop model, *Nucl. Phys. B* 814 (2009) 461–484.
- [26] B. Nienhuis, Critical behavior of two-dimensional spin models and charge asymmetry in the Coulomb gas, *J. Stat. Phys.* 34 (1984) 731–761.
- [27] G. M. Zhang and C. Z. Yang, Cluster Monte Carlo dynamics for the antiferromagnetic Ising model on a triangular lattice, *Phys. Rev. B* 50 (1994) 12546–12549.
- [28] P. D. Coddington and L. Han, Generalized cluster algorithms for frustrated spin models, *Phys. Rev. B* 50 (1994) 3058–3067.
- [29] R. J. Baxter, Colorings of a Hexagonal Lattice, *J. Math. Phys.* 11 (1970) 784–789.
- [30] Jian-Sheng Wang, R. H. Swendsen and R. Kotecký, Three-state antiferromagnetic Potts models: A Monte Carlo study, *Phys. Rev. B* 42 (1990) 2465–2474.
- [31] Bojan Mohar and Jesús Salas, A new Kempe invariant and the (non)-ergodicity of the WSK algorithm, *J. Phys. A: Math. Theor.* 42 (2009) 225204.
- [32] Bojan Mohar and Jesús Salas, On the non-ergodicity of the Swendsen-Wang-Kotecký algorithm on the kagomé lattice, *J. Stat. Mech.* 2010 (2010) 05016.
- [33] N. Prokof'ev and B. Svistunov, Worm Algorithms for Classical Statistical Models, *Phys. Rev. Lett.* 87 (2001) 160601.
- [34] Youjin Deng, Timothy M. Garoni and Alan D. Sokal, Dynamic Critical Behavior of the Worm Algorithm for the Ising Model, *Phys. Rev. Lett.* 99 (2007) 110601.
- [35] W. Janke, T. Neuhaus and A. M. J. Schakel, Critical loop gases and the worm algorithm, *Nucl. Phys. B* 829 (2010) 573–599.
- [36] U. Wolff, Simulating the all-order strong coupling expansion III: $O(N)$ sigma/loop models, *Nucl. Phys. B* 824 (2010) 254–272.
- [37] R. Diestel, *Graph Theory*, 3rd Edition, Springer-Verlag, New York, 2005.
- [38] R. J. Baxter, q colourings of the triangular lattice, *J. Phys. A: Math. Gen.* 19 (1986) 2821–2839.
- [39] R. J. Baxter, Chromatic polynomials of large triangular lattices, *J. Phys. A: Math. Gen.* 20 (1987) 5241–5261.
- [40] M. T. Batchelor and H. W. J. Blöte, Conformal anomaly and scaling dimensions of the $O(n)$ model from an exact solution on the honeycomb lattice, *Phys. Rev. Lett.* 61 (1988) 138–140.
- [41] M. T. Batchelor and H. W. J. Blöte, Conformal invariance and critical behavior of the $O(n)$ model on the honeycomb lattice, *Phys. Rev. B* 39 (1989) 2391–2402.
- [42] J. Suzuki, Finite Size Correction and Conformal Anomaly for $O(n)$ Spin System, *J. Phys. Soc. Jpn* 57 (1988) 2966–2975.
- [43] B. Nienhuis, Exact Critical Point and Critical Exponents of $O(n)$ Models in Two Dimensions, *Phys. Rev. Lett.* 49 (1982) 1062–1065.
- [44] H. W. J. Blöte and B. Nienhuis, Fully Packed Loop Model on the Honeycomb Lattice, *Phys. Rev. Lett.* 72 (1994) 1372–1375.
- [45] M. T. Batchelor, J. Suzuki and C. M. Yung, Exact Results for Hamiltonian Walks from the Solution of the Fully Packed Loop Model on the Honeycomb Lattice, *Phys. Rev. Lett.* 73 (1994) 2646–2649.
- [46] J. Kondev, J. de Gier and Bernard Nienhuis, Operator spectrum and exact exponents of the fully packed loop model, *J. Phys. A: Math. Gen.* 29 (1996) 6489–6504.
- [47] B. Nienhuis, Locus of the tricritical transition in a 2-dimensional q -state Potts-model, *Physica A* 177 (1991) 109–113.
- [48] J. L. Jacobsen, Unbiased Sampling of Globular Lattice Proteins in Three Dimensions, *Phys. Rev. Lett.* 100 (2008) 118102.
- [49] R. Oberdorf, A. Ferguson, J. Jacobsen and J. Kondev, Secondary structures in long compact polymers, *Phys. Rev. E* 74 (2006) 051801.
- [50] M. L. Mansfield, Monte Carlo studies of polymer chain dimensions in the melt, *J. Chem. Phys.* 77 (1982) 1554.
- [51] J. Holm, K. de Lichtenberg and M. Thorup, Poly-Logarithmic Deterministic Fully-Dynamic Algorithms for Connectivity, Minimum Spanning Tree, 2-Edge, and Biconnectivity, *J. ACM* 48 (2001) 723–760.

- [52] Youjin Deng, Wei Zhang, Timothy M. Garoni, Alan D. Sokal and Andrea Sportiello, Some geometric critical exponents for percolation and the random-cluster model, *Phys. Rev. E* 81 (2010) 020102(R).
- [53] J. L. Jacobsen and J. Vannimenus, Finite average lengths in critical loop models, *J. Phys. A: Math. Gen.* 32 (1999) 5455–5468.
- [54] H. Saleur and B. Duplantier, Exact determination of the percolation hull exponent in two dimensions, *Phys. Rev. Lett.* 58 (1987) 2325–2328.
- [55] B. Duplantier and H. Saleur, Exact Fractal Dimension of 2D Ising Clusters, *Phys. Rev. Lett.* 63 (1989) 2536–2536.
- [56] H. Kunz and F. Y. Wu, Exact results for an $O(n)$ model in two dimensions, *J. Phys. A: Math. Gen.* 21 (1988) L1141–L1144.